To Appear in ApJ, 670, 206
Preprint typeset using LaTeX style emulateapj v. 10/09/06

arXiv:0707.2787v2 [astro-ph] 1 Nov 2007

THE EVOLUTION OF THE FIELD AND CLUSTER MORPHOLOGY-DENSITY RELATION FOR MASS-SELECTED SAMPLES OF GALAXIES

A. van der Wel[1], B. P. Holden[2], M. Franx[3], G.D. Illingworth[2], M. P. Postman[4], D. D. Kelson[5], I. Labbé[5], Wuyts, S.3, J. P. Blakeslee[6], H. C. Ford[1]

To Appear in ApJ, 670, 206

ABSTRACT

The Sloan Digital Sky Survey (SDSS) and photometric/spectroscopic surveys in the GOODS-South field (the Chandra Deep Field-South, CDF-S) are used to construct volume-limited, stellar mass-selected samples of galaxies at redshifts $0 < z < 1$. The CDF-S sample at $0.6 < z < 1.0$ contains 207 galaxies complete down to $M = 4{\times}10^{10}\ M_{\odot}$ (for a "diet" Salpeter initial mass function), corresponding to a luminosity limit for red galaxies of $M_{\rm B} = -20.1$. The SDSS sample at $0.020 < z < 0.045$ contains 2003 galaxies down to the same mass limit, which corresponds to $M_{\rm B} = -19.3$ for red galaxies. Morphologies are determined with an automated method, using the Sérsic parameter n and a measure of the residual from the model fits, called "bumpiness," to distinguish different morphologies. These classifications are verified with visual classifications. In agreement with previous studies, $65\% - 70\%$ of the galaxies are located on the red sequence, both at $z \sim 0.03$ and at $z \sim 0.8$. Similarly, $65\% - 70\%$ of the galaxies have $n > 2.5$. The fraction of E+S0 galaxies is $43\% \pm 3\%$ at $z \sim 0.03$ and $48\% \pm 7\%$ at $z \sim 0.8$; i.e., it has not changed significantly since $z \sim 0.8$. When combined with recent results for cluster galaxies in the same redshift range, we find that the morphology-density relation for galaxies more massive than $0.5M^*$ has remained constant since at least $z \sim 0.8$. This implies that galaxies evolve in mass, morphology, and density such that the morphology-density relation does not change. In particular, the decline of star formation activity and the accompanying increase in the stellar mass density of red galaxies since $z \sim 1$ must happen without large changes in the early-type galaxy fraction in a given environment.

Subject headings: galaxies: clusters: general—galaxies: elliptical and lenticular, cD—galaxies: evolution—galaxies: formation—galaxies: fundamental parameters—galaxies: general—galaxies: photometry

1. INTRODUCTION

The morphology-density relation (MDR; Dressler 1980), i.e., the observation that high-density environments contain a higher fraction of early-type galaxies than low-density environments, provides a clue about the formation and evolution of galaxies, and suggests that environment plays an important role in shaping the galaxy population. The interpretation of the MDR, however, is not straightforward because of additional correlations between morphology, galaxy mass, color, star formation history, and metallicity; all quantities that depend on environment (e.g., Hogg et al. 2003; Kauffmann et al. 2003, 2004; Blanton et al. 2005a; Baldry et al. 2006). There are strong indications that the stellar mass of a galaxy, independently of the environment, determines the color (Baldry et al. 2006) and concentration (Kauffmann et al. 2004) of a galaxy. In addition, the environment plays a role in star formation activity (Kauffmann et al. 2004).

It is a matter of debate whether the fate of a galaxy is ultimately determined by its mass or its environment. Studies of galaxy properties such as those mentioned above at higher redshifts help to answer those questions, and there is abundant evidence for both scenarios. The massive galaxy populations of $z \sim 1$ clusters appear to be fully assembled and passively evolving (e.g., De Propris et al. 2007), whereas the galaxy population as a whole undergoes significant evolution between $z = 1$ and the present, both in terms of mass and color (e.g., Bell et al. 2004b) and in terms of star formation (e.g., Le Floc'h et al. 2005). This points to a strong relation between formation epoch and environment. On the other hand, high-mass galaxies have had lower specific star formation rates than low-mass galaxies since at least $z \sim 2$ (e.g., Juneau et al. 2005; Noeske et al. 2007), and there is only a very modest age difference between field and cluster early-type galaxies with masses $M > 10^{11}\ M_{\odot}$ at $z \sim 1$ (van Dokkum & van der Marel 2007), with possibly a stronger age dependence on mass than environment (van der Wel et al. 2005; Treu et al. 2005). All these results, at first sight contradictory, will have to be reconciled with each other.

The MDR, and its evolution with redshift, plays a crucial role in our understanding of the effect of the environ-

[1] Department of Physics and Astronomy, Johns Hopkins University, 3400 North Charles Street, Baltimore, MD 21218; wel@pha.jhu.edu
[2] University of California Observatories/Lick Observatory, University of California, Santa Cruz, CA 95064
[3] Leiden Observatory, Leiden University, P.O.Box 9513, NL-2300 AA Leiden, Netherlands
[4] Space Telescope Science Institute, 3700 San Martin Drive, Baltimore, MD 21218
[5] Carnegie Observatories, Carnegie Institution of Washington, 813 Santa Barbara Street, Pasadena, CA 91101
[6] Department of Physics and Astronomy, Washington State University, Pullman, WA 99163-2814
[7] Based on observations with the *Hubble Space Telescope*, obtained at the Space Telescope Science Institute, which is operated by AURA, Inc., under NASA contract NAS5-26555, and observations made with the *Spitzer Space Telescope*, which is operated by the Jet Propulsion Laboratory, California Institute of Technology, under NASA contract 1407.

ment on galaxy evolution, and significant evolution of the early-type galaxy fraction has been found between $z \sim 1$ and the present (e.g., Dressler et al. 1997; Smith et al. 2005; Postman et al. 2005). These studies are based on samples that are selected by luminosity, and to ensure that the $z \sim 1$ samples contain the progenitors of the galaxies in the local samples, the luminosity limit for samples at different redshifts is corrected for evolution. It is assumed that the evolution is the same for all galaxies, which might not be the case. In addition, luminosity is very sensitive to bursts of star formation that are likely far more prevalent at $z \sim 1$ than in the local universe. Therefore, it is worthwhile to adopt an alternative selection method that is less sensitive to potentially rapidly changing galaxy properties such as the star formation rate. Stellar mass is a quantity that changes less rapidly than luminosity, such that it might be a more suitable tracer of the $z \sim 1$ progenitors of local galaxies. In addition, it is more straightforward to compare stellar masses to model predictions. Obviously, mass is not an ideal tracer of the evolving galaxy population, just like luminosity, as it increases through star formation and mergers. Still, in Holden et al. (2007, , hereafter Paper I) we show that there is no discernible evolution between $z = 0.83$ and the present in the morphological mix of galaxies that are more massive than $4 \times 10^{10}\ M_{\odot}$ ($\sim$25% of the mass of a typical cluster galaxy, $\sim$50% of the mass of a typical field galaxy). The evolution in the early-type fraction seen in luminosity-selected samples of cluster galaxies is due to the relative increase in the number of blue, star-forming, low-mass galaxies.

Given the abundant evidence for significant evolution since $z \sim 1$ in the galaxy population outside clusters, it is important to measure the early-type galaxy fraction at lower densities. It is not inconceivable that the early-type galaxy fraction does evolve strongly in those environments because of the strong evolution of the galaxy population in the field and in groups. On the other hand, if morphological evolution is primarily driven by environmental effects, the morphological mix of the galaxy population in a given density might not evolve. Several authors have studied the morphological mix of galaxies at $z \sim 1$ (e.g., Bell et al. 2004a; Bundy et al. 2005; Capak et al. 2007; Abraham et al. 2007). A range of techniques and sample selection methods is used in those investigations, and it is not always clear how the high-z results compare to local studies and how sample selection affects the interpretation. In particular, mass estimates and morphologies are generally not obtained with the same method for local and distant galaxy samples, such that systematic errors may contribute to the observed evolution in, for example, the early-type fraction.

In this paper we construct mass-selected samples of low- and high-redshift galaxies with morphologies classified in an internally consistent manner, such that the morphological mix of the galaxy population at low and high redshift can be directly compared both with each other and with our recent results on samples of cluster galaxies over the same redshift range (Paper I). In § 2 we describe our galaxy samples extracted from the Sloan Digital Sky Survey (SDSS) at redshifts $0.020 < z < 0.045$ and the Chandra Deep Field-South (CDF-S) at redshifts $0.6 < z < 1.0$ and determine galaxy masses and morphologies. In § 3 we present and discuss our results and their implications for the evolution of the early-type galaxy fraction in our field samples and, through comparison with cluster galaxies, how the MDR evolves with redshift. Finally, in § 4 we put our results in the context of the evolving red sequence and the decline in the average cosmic star formation rate density. We adopt the standard cosmological parameters, $(\Omega_{\rm M},\ \Omega_{\Lambda},\ h) = (0.3,\ 0.7,\ 0.7)$.

2. DATA

First, we construct a complete, stellar-mass-selected, volume-limited sample of galaxies at redshifts $0.02 < z < 0.045$ from the Sloan Digital Sky Survey (SDSS; York et al. 2000), Data Release 5 (DR5; Adelman-McCarthy et al. 2007). Similarly, we construct a stellar mass-selected, volume-limited sample at $0.6 < z < 1.0$ in the Chandra Deep Field-South (CDF-S). Then we determine the morphologies of the galaxies in both samples in a consistent manner and quantify the environment (parameterized by the local surface galaxy density) in which the galaxies are situated.

2.1. *A Mass-Selected, Volume-Limited SDSS Galaxy Sample*

The sample consists of two redshift bins: galaxies at redshifts $0.02 < z < 0.03$ with stellar masses $4 \times 10^{10} < M/M_{\odot} < 1.6 \times 10^{11}$, and galaxies at redshifts $0.035 < z < 0.045$ with stellar masses $M > 1.25 \times 10^{11}\ M_{\odot}$. The reason for this split is to ensure spectroscopic completeness on both the faint and the bright end and to minimize systematic problems with the photometry of bright galaxies (see below). The g-band magnitudes of the galaxies in these samples range from $g_{\rm mod} = 13.7$ to 16.5. Here $g_{\rm mod}$ is the model magnitude from the SDSS pipeline (see below for the definition). The upper limit $g_{\rm mod} = 13.7$ ensures that this sample is not incomplete due to the cutoff at bright magnitudes in the SDSS spectroscopic survey (Strauss et al. 2002). This source of incompleteness is essentially a surface brightness limit imposed to avoid saturation. The lower magnitude limit $g_{\rm mod} = 16.5$ ensures spectroscopic completeness at the faint end (Blanton et al. 2005b) and the feasibility of determining morphologies without being limited by background noise. Finally, only those galaxies located at least 130 pixels from the edge of the image tiles are included in the sample, in order to avoid problems with the morphological analysis described below. This does not introduce systematic effects other than decreasing the volume of the sample by 28%. The lower mass limit of $M = 4 \times 10^{10}\ M_{\odot}$ is chosen to match the $z \sim 0.8$ sample that we construct below (see § 2.2). Approximately two-thirds of the stars are located in galaxies with $M > 4 \times 10^{10}\ M_{\odot}$ (Bell et al. 2003), such that in terms of stellar mass our samples contain a representative fraction of the galaxy population.

Total magnitudes can be underestimated due to overestimation of the sky brightness by the SDSS reduction pipeline (Lauer et al. 2007). The magnitude of this effect depends on both galaxy size and surface brightness, i.e., to first order on apparent magnitude. Since we are working with a large sample we are primarily interested in a statistical, magnitude-dependent correction for the sample as a whole. For a dozen galaxies with magnitudes across the range of our sample we determine to-

TABLE 1
Magnitude and Color Conversions

z	g_0	$(u-g)_0$	$(g-r)_0$
0.02	$g-0.096(g-r)+0.019$	$1.035(u-g)-0.111$	$0.951(g-r)-0.001$
0.03	$g-0.141(g-r)+0.027$	$1.037(u-g)-0.124$	$0.928(g-r)-0.003$
0.04	$g-0.185(g-r)+0.035$	$1.029(u-g)-0.123$	$0.906(g-r)-0.005$
z	B_0	$(U-B)_0$	$(B-V)_0$
0.60	$z+0.559(v-z)+0.428$	$0.732(v-i)-0.703$	$0.501(v-z)-0.049$
0.70	$z+0.413(v-z)+0.511$	$0.696(v-i)-0.757$	$0.463(v-z)-0.075$
0.80	$z+0.289(v-z)+0.617$	$0.661(v-i)-0.778$	$0.411(v-z)-0.082$
0.90	$z+0.466(i-z)+0.792$	$0.404(v-z)-0.666$	$0.982(i-z)+0.030$
1.00	$z+0.194(i-z)+0.847$	$0.371(v-z)-0.628$	$1.044(i-z)-0.142$

Note. — Transformations used to calculate rest-frame magnitudes and colors from observed magnitudes and colors for eight different redshifts. The letters v, i, and z are shorthand for v_{606}, i_{775}, and z_{850}, respectively. The magnitudes are total magnitudes for which the definitions can be found in §§ 2.1 and 2.2. The total magnitudes g_0 and B_0 are not corrected for cosmological surface brightness dimming. Note that B_0, $(U-B)_0$, and $(B-V)_0$ are on the Vega system, whereas all other magnitudes and colors are on the AB system. The $u-g$ conversion contains a correction (-0.04 mag) to account for the difference between the SDSS u-band zero point and the true AB zero point.

tal magnitudes by hand. The true background is determined by SExtractor (Bertin & Arnouts 1996), using the global background mode, and the total flux is measured with the `ellipse` task in IRAF. We find that $g_{\rm tot} = g_{\rm mod} - 0.2(15 - g_{\rm mod})$ for $g_{\rm mod} < 15$ and $g_{\rm tot} = g_{\rm mod}$ for $g_{\rm mod} > 15$. This correction is of similar magnitude to the corrections applied by von der Linden et al. (2007), who designed a method to obtain accurate, corrected magnitudes for individual galaxies. Our correction is not perfect for individual galaxies but does provide a sufficiently accurate correction for the sample as a whole. The impact of the correction on the stellar masses that we derive below is ~ 0.1 dex for the brightest galaxies, such that even if the correction we apply is uncertain on the 50% level, the effect on the stellar masses is only 0.05 dex, which is negligible with respect to the other uncertainties on the mass estimates. The systematic error will be still lower.

We adopt $u-g = u_{\rm mod,c} - g_{\rm mod,c}$ and $g-r = g_{\rm mod,c} - r_{\rm mod,c}$ as the galaxy colors, where $u_{\rm mod,c}$, $g_{\rm mod,c}$, and $r_{\rm mod,c}$ are the model magnitudes, corrected for Galactic extinction. Here $r_{\rm mod,c}$ is either the De Vaucouleurs model magnitude or the exponential model magnitude, depending on which one fits best to the observed surface brightness profile in the r band. The best-fit radius, ellipticity, and orientation as determined in the r band are subsequently used to measure $u_{\rm mod,c}$ and $g_{\rm mod,c}$, with only the surface brightness as a free parameter (see Lupton et al. 2001, for a description of the data reduction pipeline). The colors thus obtained are therefore equivalent to the color within the r-band half-light radius.

K-corrections are not negligible, even at such low redshifts (Blanton et al. 2003). We derive $g_{\rm tot,0}$, $(u-g)_0$, and $(g-r)_0$ (g-band magnitudes, and $u-g$ and $g-r$ colors K-corrected to $z=0$) by following the technique applied to higher redshifts galaxies by Blakeslee et al. (2006), Holden et al. (2006) and Paper I. We derive linear relations between colors and magnitudes in the observed and rest frames from synthetic spectra for stellar populations from Bruzual & Charlot (2003) with a range of metallicities and star formation histories (exponentially declining star formation rates with different timescales). In Table 1 we show the transformations for redshifts $z = 0.02$, 0.03, and 0.04.

Subsequently, stellar masses are estimated using the relation between $(g-r)_0$ and M/L derived by Bell et al. (2003) for a "diet" Salpeter initial stellar mass function (IMF):

$$\log\left(\frac{M}{L_{\rm g}}\right) = 1.519(g-r)_0 - 0.499.$$

The diet Salpeter IMF (e.g., Bell et al. 2003) gives values of M/L that are 0.15 dex lower than in the standard Salpeter IMF, which is due to the flat slope for stellar masses below 0.35 $M_\odot$. The K-corrections and color-M/L conversions can be combined to give a unique relation between stellar mass, apparent magnitude, color, and redshift:

$$\log\left(\frac{M}{M_\odot}\right) = f(g_{\rm tot};(g-r);z) =$$
$$-0.399\left[g_{\rm tot} - 3.65(g-r) - 4.79\log\left(\frac{z}{0.03}\right) - 39.55\right].$$

In order to compare with previous work and the $z\sim0.8$ sample described below, we derive the standard $U-B$ and $B-V$ colors and B-band magnitudes in the Vega system.

In Figure 1 we compare our stellar mass estimates with kinematic mass estimates, where the latter is defined as $M_{\rm dyn}/M_\odot = \log(R) + 2\log(\sigma_c) + 6.07$ (Jørgensen et al. 1996). Here, R is either the De Vaucouleurs or the exponential disk scale radius in kiloparsecs as measured in the g band, depending on which profile provides the better fit, and σ_c is the aperture-corrected velocity dispersion (see Bernardi et al. 2003) in kilometers per second. There is an average, systematic offset of 0.10 dex, the stellar mass estimates being lower than the kinematic mass estimates. This can be due to the choice of the diet Salpeter IMF and/or the presence of nonbaryonic matter, even though σ is measured at the centers of the galaxies, which are dominated by stars. The offset varies slightly with mass (by $\lesssim \pm0.05$ dex) for galaxies with $M_{\rm phot} > 4\times10^{10}$ $M_\odot$, the mass limit of the sample used in this paper. Such a mass dependence of the difference between kinematic and stellar mass estimates is also seen at higher redshifts (see § 2.2). The scatter in Figure 1 is 0.17 dex, which implies that the errors in the photometric mass estimates for individual galaxies are less than

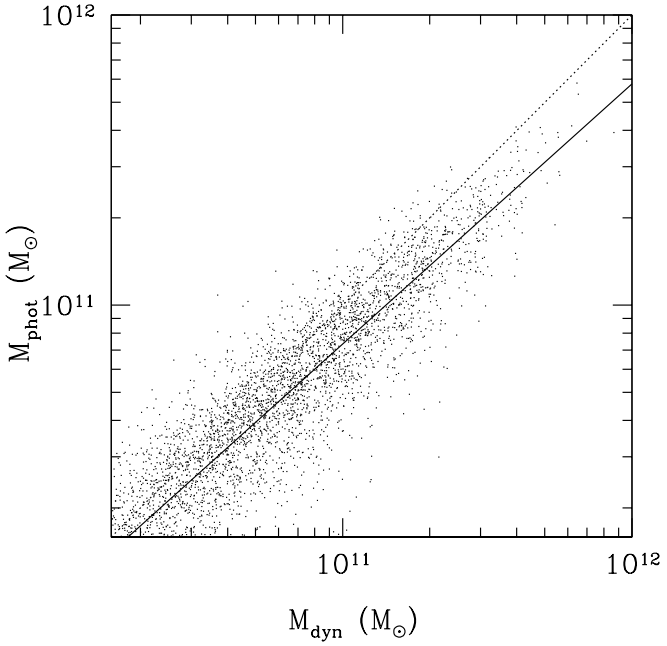


FIG. 1.— Comparison between stellar masses (as used in this paper) and kinematic masses ($\propto R\sigma^2$) for galaxies at redshifts $0.030 < z < 0.045$. The dotted line indicates the one-to-one correspondence between $M_{\rm dyn}$ and $M_{\rm phot}$. The solid line is the best linear fit, which has slope 0.9 and shows that the offset between the two mass estimates is, on average, 0.10 dex. The scatter is 0.17 dex.

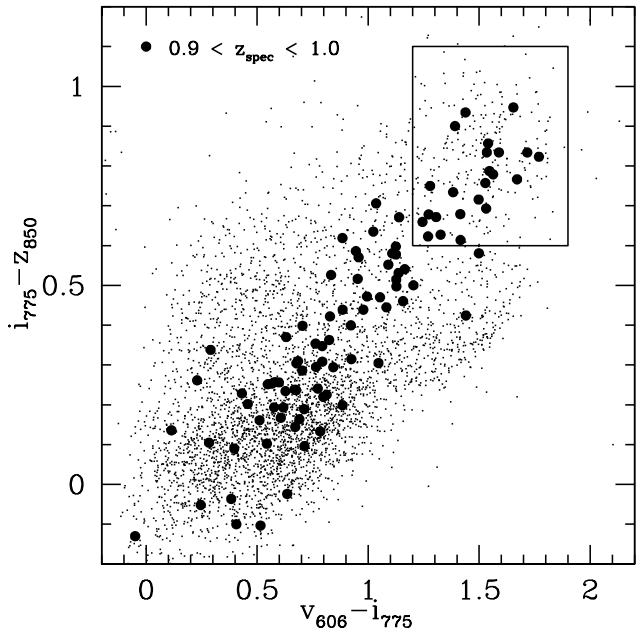


FIG. 2.— *Small circles:* Galaxies brighter than $z_{850} = 24$ in the CDF-S. *Large circles:* Galaxies with spectroscopic redshifts $0.9 < z < 1.0$. A mass-selected sample will be biased most strongly at the high-redshift end ($z = 1$) and against those galaxies with the highest M/L, i.e., those with the reddest colors. The area indicated by the rectangle indicates the colors of the reddest galaxies at $z \sim 1$. In Fig. 3 we address the redshift completeness of galaxies with such colors.

$\sim$50%. Note that this is an upper limit on the real uncertainty since kinematic mass estimates have their own uncertainties. We conclude that the color measurements and the resulting stellar mass estimates are sufficiently accurate for our purposes.

The final sample consists of 2003 galaxies that are more massive than $M = 4 \times 10^{10}\ M_\odot$. Of those, 545 are in the $0.035 < z < 0.045$ subsample of galaxies with masses $M > 1.25 \times 10^{11}\ M_\odot$. When we compute numbers and fractions of numbers of galaxies we give those high-mass galaxies lower weight (0.395), which is the ratio of the volumes occupied by the $0.035 < z < 0.045$ sample and the $0.02 < z < 0.03$ sample.

2.2. *A Mass-Selected, Volume-Limited Galaxy Sample in the CDF-S*

We combine photometric and spectroscopic redshift samples to construct a stellar mass-limited sample of galaxies in the CDF-S in the redshift range $0.6 < z < 1.0$. We use the photometric redshift catalog by Wuyts et al. (2007), which is based on a K-band-selected sample. We supplement these with spectroscopic redshifts from the literature (Le Fèvre et al. 2004; Mignoli et al. 2005; van der Wel et al. 2005; Vanzella et al. 2006). Only those galaxies for which the spectroscopic redshifts have been measured with reasonable confidence (best or second-best quality flags) are considered. Of the final sample, 142 out of 207 or 69% have spectroscopic redshifts. We refer to the respective publications for explanations of the confidence indicators.

Extensive comparisons by Wuyts et al. show that in the redshift range of our sample, there are no systematic differences between spectroscopic and photometric redshifts, regardless of color and magnitude cuts imposed on the sample. There are occasional catastrophic failures, but their number is small ($1\% - 2\%$), and therefore this does not introduce significant systematic effects.

The K-band limit of the photometric redshift catalog determines the mass completeness limit of our sample. Since we use v_{606}-, i_{775}-, and z_{850}-band ACS (*Hubble Space Telescope* Advanced Camera for Surveys) photometry to calculate masses, luminosities, and rest-frame colors we quantify the completeness limit in terms of z_{850}-band total magnitudes. The z_{850}-band total magnitudes are the SExtractor Best magnitude, but we add flux (0.2 mag) to correct for light outside the aperture (Benítez et al. 2004; Blakeslee et al. 2006). We measure $v_{606} - i_{775}$ and $i_{775} - z_{850}$ within a $0.5''$ diameter aperture, and we correct for differential point-spread function (PSF) effects. The latter correction is negligible in $v_{606} - i_{775}$ but ranges up to 0.07 mag (for point sources) in $i_{775} - z_{850}$. The aperture is chosen such that we measure the color within the effective radius or half-light radius of a typical $z \sim 0.8$ galaxy, which corresponds closely to the model colors we use to define the colors of the galaxies in the $z \sim 0.03$ sample (see § 2.1).

Selection effects in a mass-limited sample will be strongest at the high end of a redshift bin (here $0.6 < z < 1.0$) and for the galaxies with the highest mass-to-light ratio (M/L), i.e., the reddest galaxies. In Figure 2 we show the $v_{606} - i_{775}$ and $i_{775} - z_{850}$ colors of the galaxies in the CDF-S with spectroscopic redshifts $0.9 < z_{\rm spec} < 1.0$. The rectangle, which outlines the region with the reddest galaxies at that redshift, indicates for which colors incompleteness first begins to affect our mass-limited sample. In Figure 3 we show that for those colors the K-band-selected photometric redshift catalog

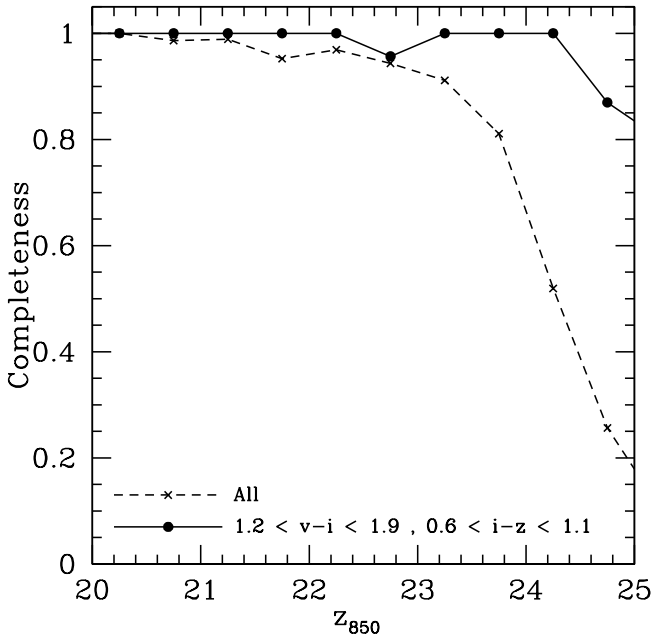


FIG. 3.— *Dashed line with crosses:* Fraction of galaxies in the CDF-S with known spectroscopic and/or photometric redshifts as a function of z_{850} magnitude. The completeness begins to decrease at $z_{850} \sim 23 - 23.5$. *Dotted line with circles:* Completeness of galaxies within the rectangle indicated in Fig. 2, i.e., those galaxies with colors similar to the reddest galaxies at $z \sim 1$. This sample is essentially complete down to $z_{850} = 24$, which implies that we can use $z_{850} = 24$ to define the mass limit of the sample.

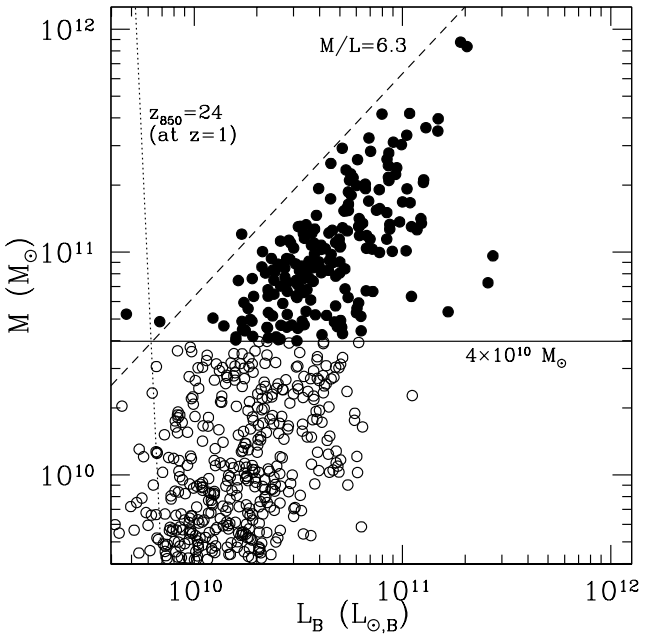


FIG. 4.— Rest-frame B-band luminosity vs. stellar mass for galaxies in the CDF-S with redshifts $0.6 < z < 1.0$, using spectroscopic redshifts if available, and, to ensure completeness, including galaxies with only photometric redshifts as well. Our magnitude completeness limit $z_{850} = 24$ corresponds to the luminosity limit at $z = 1$ (*dotted line*). In addition, we adopt $\log(M/L_B) = 0.8$ (*dashed line*) as the maximum value that the M/L of any galaxy can take. This is a reasonable assumption as this is the highest M/L for galaxies at the high-mass, high-luminosity end of our sample. The magnitude and M/L limits cross at $M > 4{\times}10^{10}\ M_{\odot}$. This is the mass completeness limit of our sample. At lower masses, our sample is incomplete for faint, red (high M/L) galaxies (see Fig. 3). The mass-selected sample contains 207 galaxies, 142 of which have spectroscopic redshifts.

is virtually complete down to $z_{850} = 24$, fainter than the completeness limit of galaxies with a typical color. In the following, we adopt $z_{850} = 24$ as the magnitude limit which we use to define the mass completeness limit of our sample. Bluer galaxies near this mass limit are much brighter, and incompleteness does not play a role for those objects. The reason for using a z_{850}-band magnitude limit to define the mass completeness limit instead of the K-band magnitude limit of the photometric redshift catalog is that we derive stellar masses by estimating mass-to-light ratios in the rest-frame B-band, which corresponds to the observed z band at $0.6 < z < 1.0$.

Stellar masses are derived with the same method as used for the $z \sim 0.03$ galaxy sample. First, observed magnitudes and colors (z_{850}, $v_{606} - i_{775}$, and $i_{775} - z_{850}$) are used to derive rest-frame B-band luminosities and rest-frame $U - B$ and $B - V$ colors. For $z < 0.85$ we use $v_{606} - i_{775}$ to derive $(U - B)_0$ and $v_{606} - z_{850}$ to derive $(B - V)_0$ and $M_{\mathrm{B},0}$; for $z > 0.85$ we use $v_{606} - z_{850}$ to derive $(U - B)_0$ and $i_{775} - z_{850}$ to derive $(B - V)_0$ and $M_{\mathrm{B},0}$. These choices optimally match the observed and rest-frame bands, and the derived rest-frame colors are well behaved as a function of redshift. Examples for various redshifts are given in Table 1. The rest-frame U-, B-, and V-band magnitudes and colors are in the Vega system, as opposed to the other magnitudes and colors, which are in the AB system. This is necessary to facilitate the comparison with earlier results. Finally, the empirical relation between M/L and $B - V$ from Bell et al. (2003) is used to estimate the stellar masses:

$$\log\left(\frac{M}{L_{\mathrm{B}}}\right)) = 1.737(B-V)_0 - 0.994.$$

For 14 early-type galaxies in the $z \sim 0.8$ sample kinematic measurements are available from van der Wel et al. (2005). There is a systematic offset between the kinematic and stellar mass estimates of 0.1 dex (the kinematic masses being larger) and a scatter of 0.3 dex. These results are consistent with earlier determinations of the robustness of stellar mass estimates at $z \sim 0.8 - 1$ (van der Wel et al. 2006; Holden et al. 2006). Most importantly, the systematic difference between kinematic and stellar mass estimates is the same (0.1 dex) for the $z \sim 0.03$ sample and the $z \sim 0.8$ sample. Therefore, we conclude that our stellar mass estimates do not introduce systematic effects into our samples that exceed 0.1 dex in mass as was found earlier by both van der Wel et al. (2006) and Holden et al. (2006). Uncertainties at that level do not significantly affect our results. The difference between the kinematic and stellar mass estimates is mass dependent (see, e.g., Holden et al. 2006, and Paper I), but since this is also the case for our $z \sim 0.03$ sample (see § 2.1), and at the same level, this does not affect our results significantly.

For late-type galaxies a comparison between kinematic and stellar mass estimates is less straightforward. Recently, Kassin et al. (2007) showed that the relation between stellar mass and kinematic mass as defined by a combination of the rotation speed and the velocity dispersion of the gas does not vary by more than ∼0.1 dex over the redshift range $0.1 < z < 1.2$. However, the stellar masses from Kassin et al. are determined by fitting

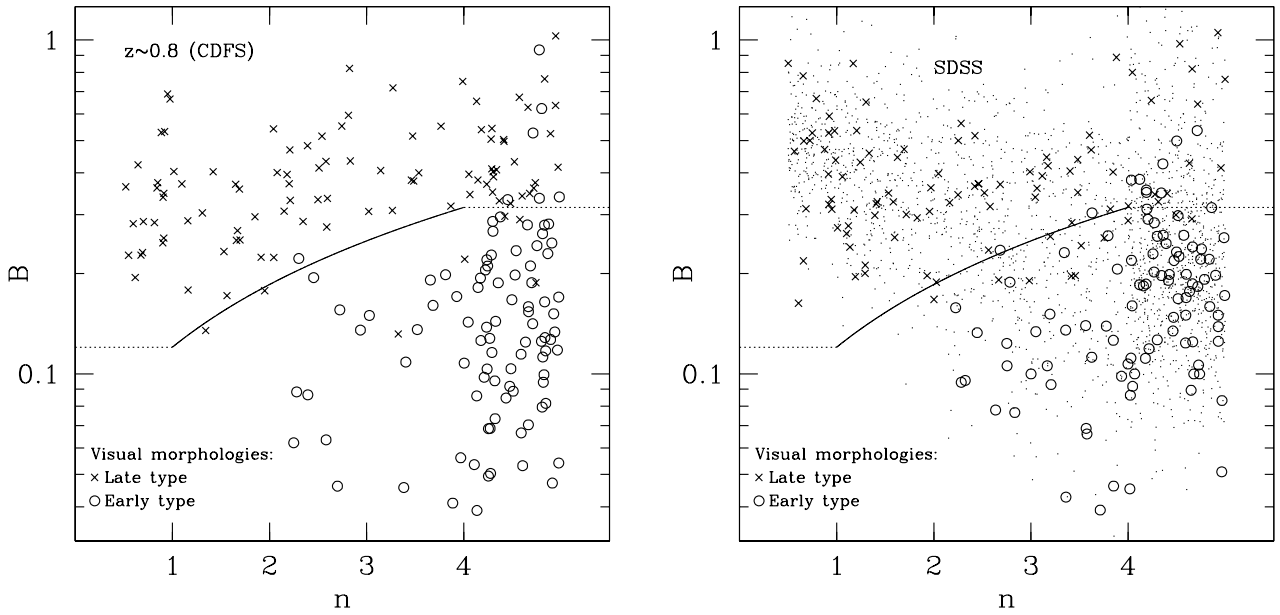


FIG. 5.— Sérsic n vs. bumpiness B for all 207 galaxies in the mass-selected $z \sim 0.8$ sample (*left*) and the 2003 galaxies in the $z \sim 0.03$ sample (*right*). The 200 galaxies with visual classifications are separately indicated, and the remainder of the sample is indicated with small dots. The Sérsic index n is restricted to be between $n = 1$ and 4, but to enhance the readability of the figure we have randomly distributed the values of n between 0.5 and 1 for galaxies with $n = 1$ and between $4 < n < 5$ for galaxies with $n = 4$. Visual classifications are indicated by different symbols: early types are indicated by open circles, late types by crosses. The curved line, $B = 0.065(n + 0.85)$, indicates the separation between early types and late types according to the $B - n$ classification. The correspondence between the visual and automated classifications is very good. See text for more details and Figure 6 for illustration.

stellar population models to broadband spectral energy distributions, which is not directly comparable with our method. If Kassin et al. had used the color-M/L relations from Bell et al. (2003), the stellar masses would have changed such that at $z \sim 1$ they would be ∼0.2 dex higher than those of local galaxies with the same kinematic mass (Paper I). We comment on the effects of possible biases where relevant.

In Figure 4 we show the rest-frame B-band luminosities and stellar masses of the galaxies in our $z \sim 0.8$ sample. The highest M/L that occurs (for luminous, red galaxies) is $M/L_{\rm B} = 6.3$. We adopt this as the M/L upper boundary, which, combined with the magnitude limit derived above ($z_{850} = 24$), gives us the mass completeness limit of our sample: $M = 4 \times 10^{10}\ M_{\odot}$ (see Fig. 4). The mass-limited sample contains 207 galaxies.

The average M/L is $M/L_{\rm B} = 2.4$ for the galaxies with $M > 4 \times 10^{10}\ M_{\odot}$. For the $z \sim 0.03$ sample this is $M/L_{\rm B} = 4.9$. This implies 0.75 mag evolution between the two samples in the B-band, or 1 mag per unit redshift. This is consistent with the evolution of L^* (e.g., Brown et al. 2007), but somewhat less than the $M/L_{\rm B}$ evolution inferred via fundamental plane analyses for $z \sim 1$ field early-type galaxies with similar masses (0.55 dex; van der Wel et al. 2005; Treu et al. 2005; van Dokkum & van der Marel 2007). This difference may contain contributions from a systematic uncertainty in the high-z mass estimates as described above, and an increased number of very red, dusty galaxies at $z \sim 1$ with high M/L.

2.3. *Morphological Classifications*

Traditionally, visual morphological classifications are used for morphological studies of high-redshift galaxy populations, for example the evolution of the MDR (e.g., Postman et al. 2005). In recent years, however, increased sample sizes have initiated the emergence of several alternative, automated classification schemes (Conselice et al. 2000; Abraham et al. 2003; Lotz et al. 2004; Blakeslee et al. 2006). In addition to the traditional, visual classifications we therefore also deploy a quantitative measure of the galaxy morphologies. This enables us to analyze the large sample of $z \sim 0.03$ galaxies and to examine, in a quantitative manner, the effect of cosmological surface brightness dimming on the detectability of disks, spiral arms, and irregularities. The visual classifications are used to verify the robustness of this automated classification method. In this paper we simply distinguish between early- and late-type galaxies, or, in the T-type classification scheme (see Postman et al. 2005), between galaxies with type $T \leq 0$ (E, E/S0, and S0) and galaxies with type $T > 0$ (Sa and later). The separation into subclasses, for example E and S0, will be investigated in a future paper.

Visual morphologies were determined by A. v. d. W. by examining the g-band images of 200 randomly chosen galaxies in the mass-selected $z \sim 0.03$ sample and the z_{850}-band images of all 207 galaxies in the $z \sim 0.8$ sample. For 35 galaxies in the $z \sim 0.8$ sample with $T \sim 0$ or peculiar morphologies M. P. also examined the images and assigned morphologies. This provides an estimate of the random uncertainty and ensures that the same threshold ($T = 0$) is adopted as in Postman et al. (2005). Based on these results, we conservatively assume a 5.5% uncertainty in the early-type galaxy fraction due to classification errors. We note that the z_{850}-band imaging with an integration time of 12,000 s and a 10σ point-source detection limit of $z_{850} = 27$ is very deep with respect to the faintest galaxies in our sample with $z_{850} = 24$. In Figure 5 we indicate early-type galaxies

with open circles and late-type galaxies with crosses.

Quantitative morphologies are determined for all galaxies with the technique outlined by Blakeslee et al. (2006), who showed that the Sérsic parameter n and bumpiness parameter B can effectively distinguish between early- and late-type galaxies. GALFIT (Peng et al. 2002) is used to fit Sérsic profiles to the g-band and z_{850}-band images; n is constrained to values between $n = 1$ and 4. The only reason for not allowing larger values of n is that the effective radii for high values of n become large and uncertain. This would strongly affect the measurement of the bumpiness B, which is the rms of the residual as measured within two effective radii. In order to reduce the effect of shot noise the residual is slightly smoothed. In addition, other objects and a circular region around the center are masked. This central region is masked out because of slight PSF mismatches and because of central, small-scale deviations from a Sérsic profile. Because of the latter effect the adopted radius is distance dependent. On visual inspection we choose a 4 pixel radius for galaxies at $z = 0.03$ in the low-z sample and a 2 pixel radius for galaxies at $z = 0.80$ in the high-z sample, both scaled inversely proportional with angular diameter distance for galaxies at different redshifts.

The advantage of the $B - n$ classification over other automated classifiers is that PSF smearing is taken into account. This is essential, in particular when redshift-dependent trends are investigated in data sets with very different photometric properties. In Figure 6 we show image cutouts and give the n and B parameters for 20 randomly selected galaxies from our $z \sim 0.0$ and 0.8 samples, in order to illustrate the correspondence between the automated classification method and their morphological appearance. The parameters n and B are shown for all galaxies with visual morphologies in Figure 5. A simple linear relation separates early- and late-type galaxies: $B = 0.065(n + 0.85)$ (Fig. 5, *solid line*). Note that these coefficients are taken from Blakeslee et al. (2006), and are not chosen to optimize the correspondence between the visual and $B - n$ classifications for these particular samples. The correspondence between our results, in particular for the $z \sim 0.03$ sample, and the results by Blakeslee et al. illustrates the power of the $B - n$ method. Once PSF smearing effects and noise properties are properly taken into account, data sets with roughly similar spatial resolution provide a unique measurement of galaxy morphology through the $B - n$ classification. This extends the conclusions from Blakeslee et al. who could not claim universality of their selection criteria because of their homogeneous data sets and the small redshift range ($z = 0.83 - 0.84$) of their samples.

The visual and $B - n$ classifications agree for 93% of the galaxies in the $z \sim 0.8$ sample (193 of 207) and for 89% of the galaxies in the $z \sim 0.03$ sample (179 of 200; see also Fig. 5). Half of the mis-classifications have n- and B-values that put them close to the criterion that separates the early types from the late types (Fig. 5, *solid line*). The disagreement can be explained by the limited signal-to-noise ratio (S/N) of the images, which shows that the true random uncertainty in the visual and $B - n$ methods is ∼4%. The other half of the disagreements are mostly due to strong, central deviations from a Sérsic profile (probably point sources) or, for several galaxies in the $z \sim 0.03$ sample, large-scale deviations from a smooth profile that our fitting method does not place within two effective radii. Despite the nonnegligible numbers of erroneous classifications (∼10%), the net difference between the two classification methods in the ratio of the numbers of early-type and late-type galaxies is less than 0.5%. This is true for both the $z \sim 0.03$ sample and the $z \sim 0.8$ sample. Hence, there is virtually no systematic difference between the visual and $B - n$ classifications for the samples as a whole.

Even though the $z \sim 0.03$ and 0.8 samples have internally consistent morphological classifications, there may be a systematic difference between the two samples, which are located at very different cosmological distances. Our morphological classifications could depend on redshift, mainly because of the lower S/N of the high-z galaxy images. Because the scales of the PSF and pixels of the SDSS and ACS data sets are very similar in terms of physical size at the sample redshifts, we can test the redshift dependence of our morphological classification. We take 50 galaxies in our sample spanning the full range in magnitude and with redshifts $0.025 < z < 0.030$, such that the SDSS pixel scale corresponds to the pixel scale of an ACS image of a galaxy at $z = 0.80$. We add noise to the g-band SDSS images, taking into account K-corrections and the relative depths of the SDSS and ACS images, and reapply our two classification methods, which gives $n_{0.80}$ and $B_{0.80}$, the values for n and B as inferred from the simulated images. In Figure 7 we compare those with the original values of n and B, and we find that neither quantity shows a systematic difference. In addition, the visual morphologies of the simulated images are not different from the original visual morphologies: all features that decide on the morphology of the $z \sim 0.03$ galaxies are still visible in the simulated $z = 0.80$ images. We conclude that our classification methods do not suffer from systematic effects that introduce significant differences between the morphologies of the $z \sim 0.03$ and $z \sim 0.8$ galaxies.

2.4. *Local Density Estimates*

Traditionally, local projected surface densities are computed by measuring the distance to the n-th nearest neighbor brighter than, for example, $M_V + 0.8z < -19.78$ (e.g., Postman et al. 2005). However, since we work with mass-selected samples in this paper, it is more consistent to measure the distance to the nth nearest neighbor that is more massive than, in this case, $M > 4 \times 10^{10}\ M_\odot$. Below we discuss the difference between the two approaches.

We derive the local galaxy densities for the 142 galaxies in our $z \sim 0.8$ sample with spectroscopic redshifts. We compute the distance to the n-th nearest neighbor with a difference in rest-frame radial velocity of $\Delta v < 1000$ km s^{-1} and more massive than $M = 4 \times 10^{10}\ M_\odot$ (or, alternatively, more luminous than $M_V + 0.8z < -19.78$). Here n is the number of galaxies with such properties in the CDF-S, with a maximum of 7. The reason for allowing n to be smaller than 7 is the limited number of galaxies at a given, spectroscopic redshift. We note that for galaxies with fewer than 7 neighbors (12 of 142 for the luminosity-limited sample, 36 of 142 for the mass-limited sample) the density estimate does not systematically change for any value $3 < n < 7$. The inferred surface densities are corrected for edge effects and for incompleteness of the spectroscopic redshift catalog,

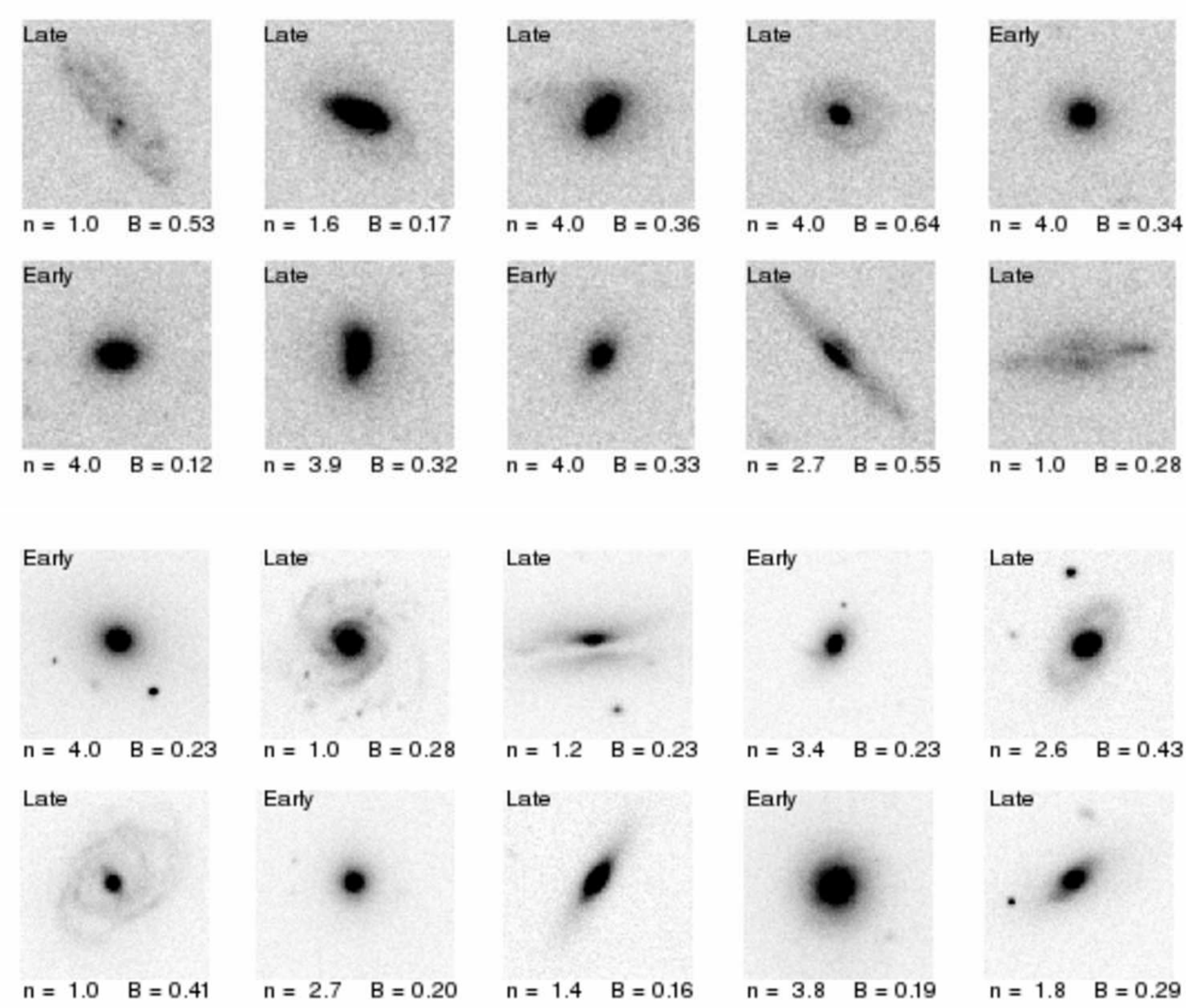


FIG. 6.— *Top two rows:* $3.4'' \times 3.4''$ z_{850}-band cutouts for 10 randomly chosen galaxies from the sample at $0.6 < z < 1.0$. *Bottom two rows:* $51'' \times 51''$ g-band cutouts for 10 randomly chosen galaxies from the sample at $z \sim 0.03$. The physical scale of both sets of images is comparable: ∼30 kpc. Visual classifications (late or early) and n and B parameters are listed for each galaxy to illustrate the correspondence between the visual morphologies and the automated classification method (see also Fig. 5).

as inferred from the spectroscopic + photometric redshift catalog.

The distributions of $\Sigma_{\rm M}$ and $\Sigma_{\rm L}$ are shown in Figure 8; $\Sigma_{\rm M}$ is typically half of $\Sigma_{\rm L}$, which is only a small difference considering the large spread (3 orders of magnitude) of densities in the samples. For galaxies with only few neighbors, the computed values are likely upper limits due to small area of the CDF-S. Obviously, for galaxies without close neighbors, the computed densities are certainly upper limits. The densities as computed here are, in principle, not directly comparable with the computations for galaxies in cluster environments (Postman et al. 2005) as those use a wider redshift range to search for neighbors to compensate for the large velocity dispersion of the cluster members. A systematic difference of up to a factor of 2 may be expected due to the difference in bin width. However, since the environments under consideration have a range in density of several orders of magnitude this does not compromise our inferences.

In a method analogous to that used for the $z \sim 0.8$ sample, we also compute local galaxy densities by finding the distance to the seventh nearest neighbor with $M = 4 \times 10^{10}\ M_{\odot}$ (or $M_{\rm V} + 0.8z < -19.78$) and $\Delta v < 1000$ km s^{-1} for each galaxy in the $z \sim 0.03$ sample. The spectroscopic survey is 100% complete at these magnitudes, therefore corrections are not needed. The distribution of Σ is shown in Figure 8. As is the case for the $z \sim 0.8$ sample, $\Sigma_{\rm M}$ and $\Sigma_{\rm L}$ typically differ by a factor of 2 for the $z \sim 0.03$ sample (see Table 1).

There is a difference of ∼0.7 dex between the median values of Σ for the $z \sim 0.03$ and 0.8 samples. This is mainly because we use the angular diameter distance $D_{\rm A}$ to calculate the physical distances between the galaxies, and not the transverse co-moving distance $D_{\rm M} = D_{\rm A}(1+z)$. This provides, to first order, redshift-independent values of the local density for bound systems

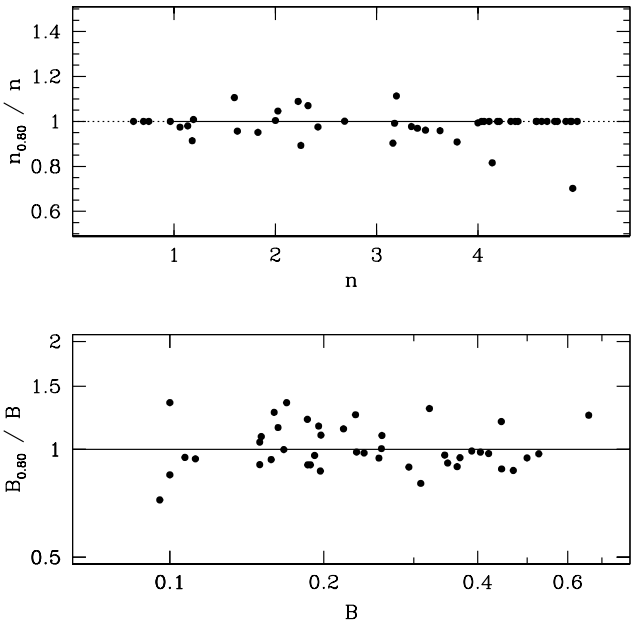


FIG. 7.— Sérsic parameter n and bumpiness parameter B for 50 galaxies at redshifts $0.025 < z < 0.030$ as determined from the original SDSS g-band images vs. the difference between n and B as determined from simulated $z = 0.80$ z-band images of the same galaxies and the original values. There are no systematic differences between the original low-z and simulated high-z morphological indicators, which indicates that the morphologies as determined for our $z \sim 0.03$ and ~ 0.8 samples are not systematically different.

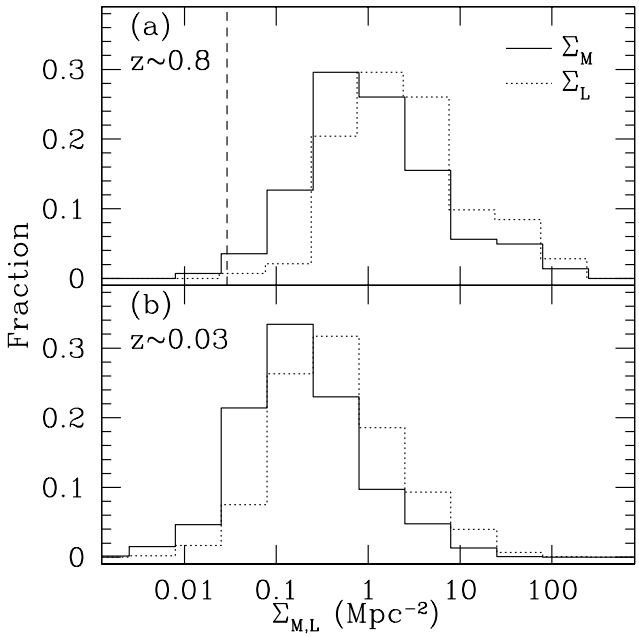


FIG. 8.— Distribution of local surface densities of the galaxies in our samples. (a) Distribution of the $0.6 < z < 1.0$ sample, where the vertical dashed line indicates the value of Σ corresponding to one galaxy within the area covered by the survey data: objects with values of Σ close to this line should be regarded as upper limits. (b) Same as (a), but for the $0.015 < z < 0.045$ sample. The solid histograms show the distributions of $\Sigma_{\rm M}$, the surface density as determined by regarding neighbors that are more massive than $M = 4 \times 10^{10}$ $M_\odot$. The dotted histograms show the distributions of $\Sigma_{\rm L}$, the surface density as determined by regarding neighbors that are brighter than $M_{\rm V} + 0.8z = -19.78$.

such as clusters, but for expansion-dominated regions the density will be redshift dependent. Using $D_{\rm M}$ would provide a redshift-independent measurement of the density and would lower the $z \sim 0.8$ densities by 0.5 dex with respect to the $z \sim 0.03$ densities. This demonstrates that the galaxies in both samples are located in similar (co-moving) environments, besides an average, apparent over-density of a factor of $1.5 - 2$ in the CDF-S which has been noted before (e.g., Bundy et al. 2005). This difference is not of great interest for this study since we consider a range in density that spans several orders of magnitude (see § 3.2). Since we are interested in the properties of the galaxy population as a function of physical density, and to facilitate the comparison with work on cluster galaxies, we use Σ as calculated with $D_{\rm A}$ in the remainder of this paper.

3. THE EVOLUTION OF THE EARLY-TYPE GALAXY FRACTION AND THE MORPHOLOGY-DENSITY RELATION

In § 3.1 we calculate the evolution of the early-type galaxy fraction in our field samples. In § 3.2 we compare this with samples of cluster galaxies over the same redshift range and determine the evolution of the MDR.

3.1. *The Field Early-Type Galaxy Fractions at $z \sim 0.8$ and 0*

Our $z \sim 0.03$ sample consists of 2003 galaxies, the $z \sim 0.8$ sample of 207 galaxies. These volume-limited samples are complete down to a stellar mass limit of $M = 4 \times 10^{10}$ $M_\odot$, about half of the typical mass of a local field galaxy, or $M_{\rm B} \sim -20.1$ for red galaxies in the $z \sim 0.8$ sample. This luminosity limit for red galaxies is similar to the $z = 0.8 - 1$ luminosity limits of the COMBO-17 (Bell et al. 2004b), DEEP2 (Faber et al. 2007) and NDWFS (Brown et al. 2007) data sets used for recent red-sequence studies.

The early-type galaxy fraction at $z \sim 0.8$, for galaxies that are more massive than $M = 4 \times 10^{10}$ $M_\odot$, is $f_{\rm ET} = 0.48 \pm 0.07$. This is based on the quantitative morphological classification method described above, but we find the same if we use the visual classifications (see also § 2.3). If only galaxies with spectroscopic redshifts are included (142 of 207 have spectroscopic redshifts), we find $f_{\rm ET} = 0.52$. The reason that the spectroscopic sample has a slightly, but not significantly, higher early-type galaxy fraction is that several of the spectroscopic campaigns specifically targeted red objects.

The main contributor to the error of 0.07 is the uncertainty in the morphological classifications (0.055). The second main source of uncertainty is Poisson noise due to the limited sample size (0.036). Smaller contributions include errors in photometric redshifts, color transformations, and M/L estimation. All these individual contributions are added in quadrature to obtain 0.07.

The early-type fraction at $z \sim 0.03$, for galaxies that are more massive than $M = 4 \times 10^{10}$ $M_\odot$, is $f_{\rm ET} = 0.43 \pm 0.03$. Essentially, the only significant contributor to the error is the uncertainty in the morphological classifications, which is slightly smaller than for the $z \sim 0.8$ sample because of the higher S/N of the images.

The early-type galaxy fractions in the mass-selected $z \sim 0.03$ and 0.8 samples are not significantly different (see Table 1 and Figure 9). This implies that if only two morphological classes are considered, then the mor-

TABLE 2
SAMPLE CHARACTERISTICS

z (1)	N (2)	f_{ET} (%) (3)	f_{RS} (%) (4)	$f_{n>2.5}$ (%) (5)	Med(Σ_M) Mpc^{-2} (6)	Med(Σ_L) Mpc^{-2} (7)	Med($U-B$) (8)	$<$ SFR $>$ $M_\odot$ yr (9)	Med(SFR) $M_\odot$ yr (10)
$0.020 < z < 0.045$	2003	43 ± 3	68 ± 1	64 ± 2	0.17	0.4	0.40	3.1 ± 1.5	0.4 ± 0.2
$0.6 < z < 1.0$	207	48 ± 7	64 ± 3	72 ± 4	1.0	2.1	0.23	12 ± 6	$\lesssim 3$

NOTE. — Col. (1) Redshift. Col. (2) Number of galaxies in the sample. Col (3) Early-type galaxy fraction as inferred from the automated $B-n$ classifications (see § 2.3). Col. (4) Fraction of galaxies located on the red sequence as defined in § 4.2. Col. (5) Fraction of galaxies with Sersic n parameter larger than $n = 2.5$ (§ 2.3). Col. (6) Median local surface density of galaxies with masses $M > 4 \times 10^{10}$ $M_\odot$ (see § 2.4). Col. (7) Median local surface density of galaxies with luminosities $M_V + 0.8z < -19.78$ (see § 2.4). Col. (8) Median rest-frame $U-B$ color as computed in §§ 2.1 and 2.2. Col. (9) Mean SFR (§ 4.1); (9) Median SFR (§ 4.1). The errors on the SFRs are assumed to be 50%, mainly to account for systematic uncertainties.

phological composition of the galaxy population did not change significantly between $z \sim 0.8$ and the present, at least above our mass limit of $M = 4 \times 10^{10}$ $M_\odot$. If anything, the early-type fraction is higher at $z \sim 0.8$ than at $z \sim 0.03$.

3.2. *Comparison with Cluster Galaxies: The Morphology-Density Relation*

As we described above, the early-type galaxy fraction in our field samples is $40\% - 50\%$ at redshifts $0 < z < 1$. In Figure 9 we compare this with the results from Paper I, where we measure the evolution of the cluster early-type fraction for galaxies down to the same mass limit ($M = 4 \times 10^{10}$ $M_\odot$) and over the same redshift range. For galaxies more massive than $M = 4 \times 10^{10}$ $M_\odot$ the early-type galaxy fraction is constant with redshift, both in the field and in massive clusters (see Fig. 9). The same MDR exists at $z = 0$ and 0.8, with early-type fractions of $40\% - 50\%$ in low-density environments and $>80\%$ in high-density environments.

The cluster samples from Paper I consist of galaxies with local densities > 50 Mpc^{-2}, our field samples consist of galaxies with densities < 50 Mpc^{-2}. In Figure 10 we show the MDR at redshifts $z \sim 0.03$ and ~ 0.8. In this figure we split our $z \sim 0.03$ field sample of 2003 galaxies into five density bins, ranging from 0.01 to 10 Mpc^{-2}. Our $z \sim 0.8$ field sample is represented by a single data point, because of the limited sample size. The average logarithm of the density of the 142 galaxies with spectroscopic redshifts is used to estimate the density for the sample as a whole. The MDR has not evolved significantly since $z \sim 0.8$ for galaxies more massive than $M = 4 \times 10^{10}$ $M_\odot$. The early-type galaxy fraction in regions with a given local density has remained constant over the past $\sim$7 Gyr.

At first sight, this result seems to be at odds with previous studies that reported significant evolution of the early-type galaxy fraction (Smith et al. 2005; Postman et al. 2005). However, those analyses are based on luminosity-selected samples, and, as is shown in Paper I, the observed evolution is driven by blue, star-forming, low-mass galaxies. Samples that are complete in terms of stellar mass do not show evidence for evolution in the early-type fraction. The evolution in the early-type fraction seen in luminosity-selected samples is driven by the evolution of the fraction of S0 galaxies, whereas the fraction of E galaxies is roughly constant (Dressler et al. 1997; Treu et al. 2003; Postman et al. 2005; Desai et al. 2007). It remains to be seen how the relative fractions of E and S0 galaxies evolve in mass-selected samples.

The MDR in the $z \sim 0.03$ data set shown in Figure 10 suggests that the early-type fraction is low ($\sim$40%) for all local surface densities $\Sigma_M \lesssim 1$ Mpc^{-2}. The transition to very high early-type fractions ($\sim$100%) happens at 1 Mpc^{-2} $< \Sigma_M <$ 100 Mpc^{-2}. This suggests that there is a critical density above which galaxies are progressively more likely to undergo morphological transformations, as was earlier noted by Goto et al. (2003). Despite the small area and the small dynamic range in densities, there is evidence for this transition in our $z \sim 0.8$ sample: if we take the galaxies with spectroscopic redshifts in the highest 20th percentile of the density distribution (typically, $\Sigma_M \sim 30$ Mpc^{-1}), we find an early-type fraction of $f_{ET} = 0.8 \pm 0.1$; for galaxies in the lowest 20th percentile (typically, $\Sigma_M \sim 0.2$ Mpc^{-1}), we find $f_{ET} = 0.4 \pm 0.1$. Without over-emphasizing these num-

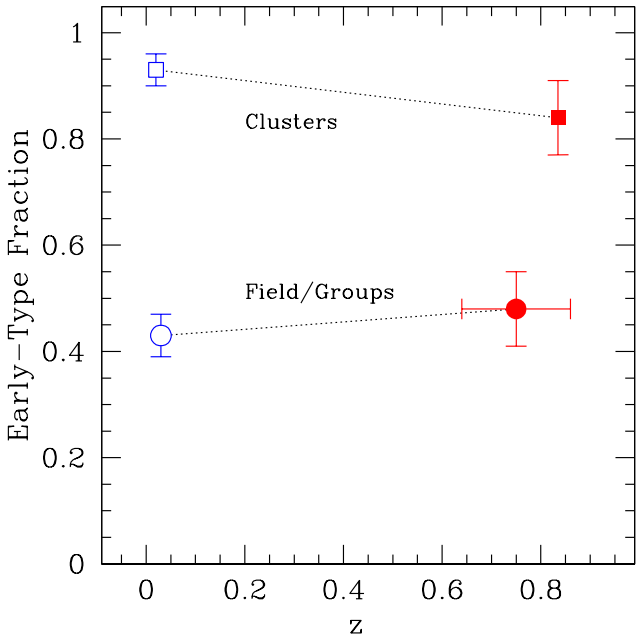


FIG. 9.— Early-type galaxy fraction as a function of redshift. The circles indicate our samples of field galaxies ($\Sigma \lesssim 50$ Mpc^{-2}) at $z \sim 0.03$ (*open blue circle*) and $z \sim 0.8$ (*filled red circle*). The squares indicate the samples of cluster galaxies ($\Sigma > 50$ Mpc^{-2}) from Paper I at $z = 0.02$ (*open blue square*, representing the Coma Cluster) and $z = 0.83$ (*filled red square*, representing the CL 0152 and MS 1054 clusters). The fraction of early-type galaxies has not changed significantly since $z \sim 0.8$ for galaxy populations in similar environments.

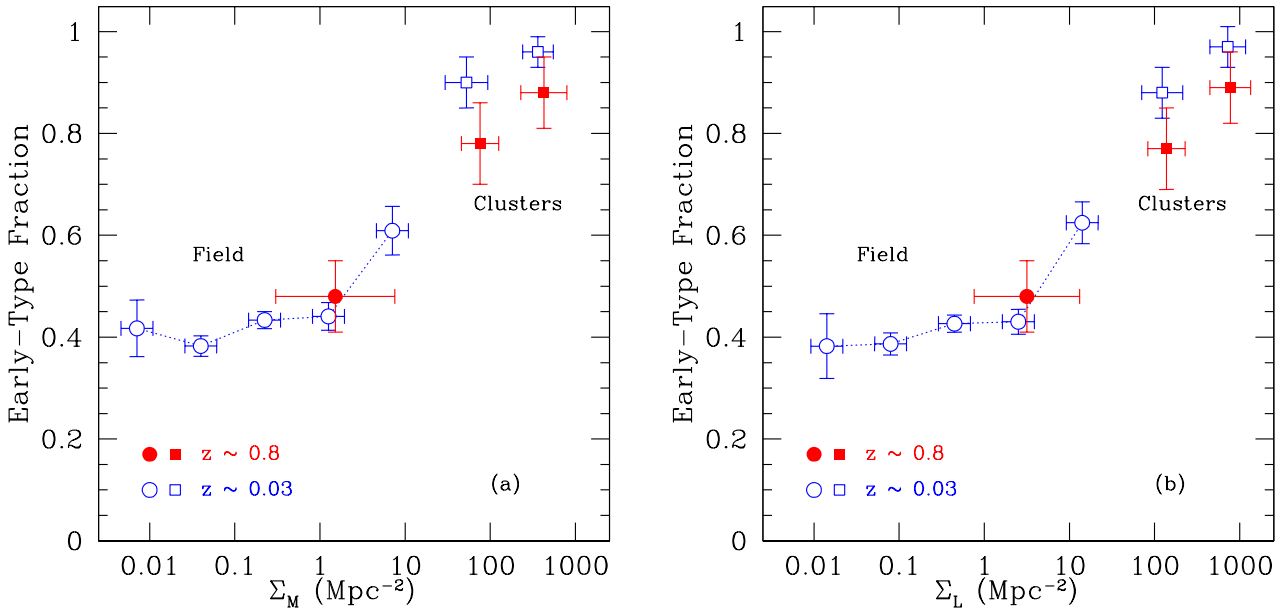


FIG. 10.— Morphology-density relation for mass-selected galaxies ($M > 4 \times 10^{10}\ M_{\odot}$) at $z \sim 0$ and $z \sim 0.8$. The symbols are the same as in Figure 9. Our $z \sim 0.03$ field sample (*open blue circles connected by the dotted line*) have been split into five density bins. Over almost 3 orders of magnitude in density the morphology-density relation has been in place since at least $z = 0.8$ and has not evolved within the measurement errors. The difference between the two panels is the use of $\Sigma_{\rm M}$ (the surface density of galaxies more massive than $M = 4 \times 10^{10}\ M_{\odot}$, or $\sim 0.5 M_{*}$) in (*a*), and the use of $\Sigma_{\rm L}$ (the surface density of galaxies more luminous than $M_{\rm V} + 0.8z < -19.78$, or $\sim 0.5 L_{*}$) in (*b*). Other than a shift of 0.3 dex in density the use of $\Sigma_{\rm M}$ and $\Sigma_{\rm L}$ is interchangeable.

bers because the sub-sample with spectroscopic redshifts is not necessarily representative of the whole $z \sim 0.8$ sample, we do note that these values follow the same trend as seen in the $z \sim 0.03$ sample (see Fig. 10).

4. DISCUSSION

4.1. *The Evolution of the Star Formation Rate*

Our conclusion that for galaxies with masses $M > 4 \times 10^{10}\ M_{\odot}$ the early-type galaxy fraction has not significantly changed in any environment over the past 7 Gyr has to be reconciled with the well-constrained decrease of the star formation rate (SFR) density by an order of magnitude since $z \sim 1$ (see, e.g., Madau et al. 1996; Wolf et al. 2003; Le Floc'h et al. 2005; Bell et al. 2005; Pérez-González et al. 2005; Zheng et al. 2006). It may seem counter-intuitive to have the SFR decrease rapidly without a change in the morphological mix of the galaxy population. On the other hand, a non-changing early-type galaxy fraction does not necessarily imply that the galaxy population itself does not evolve. Below we investigate the star formation activity in our samples.

We use the very deep, publicly available GOODS[8] 24 μm imaging from the Multiband Imaging Photometer for *Spitzer* (MIPS; Rieke et al. 2004) to verify the star formation activity in our $z \sim 0.8$ sample of mass-selected galaxies. Total 24 μm fluxes are measured by fitting the MIPS PSF to the positions of objects detected in the 3.6 μm band of the Infrared Array Camera (IRAC; Fazio et al. 2004) on board *Spitzer*. This technique reduces the effect of blending and allows for more accurate photometric measurements (for more details, see Wuyts et al. 2007). The 24 μm flux is used to estimate the bolometric infrared luminosity $L_{\rm IR}$ via the conversions from Chary & Elbaz (2001). Subsequently, we use $L_{\rm IR}$ to estimate the SFR (Kennicutt 1998), where the SFR is scaled down by 0.15 dex to account for the difference between the standard Salpeter IMF and the diet Salpeter IMF that we use. For more details concerning the K-correction and uncertainties (roughly a factor of 2 in the SFR) we refer to van der Wel et al. (2007). We conservatively use 50 μJy as the flux limit, as at lower flux levels the poor constraint on the positions of 24 μm sources requires verification of the optical counterpart for each individual object, which is beyond the scope of this paper.

In Figure 11 we show the SFR and the SFR per unit stellar mass, the specific SFR, as a function of rest-frame $U - B$ color for the 187 (of 207) $z \sim 0.8$ galaxies with MIPS coverage. Of the early-type galaxies, 11% are detected at 50 μJy, at least half of which are likely active galactic nuclei (van der Wel et al. 2007). Of the late-type galaxies, 76% have fluxes > 50 μJy, the majority of which are most likely due to star formation. The typical SFR of a late-type galaxy is $\sim 20\ M_{\odot}\ {\rm yr}^{-1}$, whereas that of an early type is $\lesssim 5\ M_{\odot}\ {\rm yr}^{-1}$. The specific SFRs are $\lesssim 10^{-10}\ {\rm yr}^{-1}$ for early types and $\lesssim 10^{-9}\ {\rm yr}^{-1}$ for late types. These values imply an increase in stellar mass of less than 10% per Gyr for the early-type galaxies and up to 100% for the late types (see Fig. 11). These findings are consistent with the work by Bell et al. (2005), who show that the star formation activity at $z \sim 0.7$ is mainly due to star formation in normal spiral galaxies with masses $> 2 \times 10^{10}\ M_{\odot}$.

Brinchmann et al. (2004) derived SFRs for galaxies in the SDSS by modeling their optical emission lines. The most robust determination of the SFR for nearby galaxies such as those in our $z \sim 0.03$ sample is that measured

[8] The Great Observatories Origins Survey (GOODS) data are available at http://data.spitzer.caltech.edu/popular/goods/Documents/goods_dr3.html

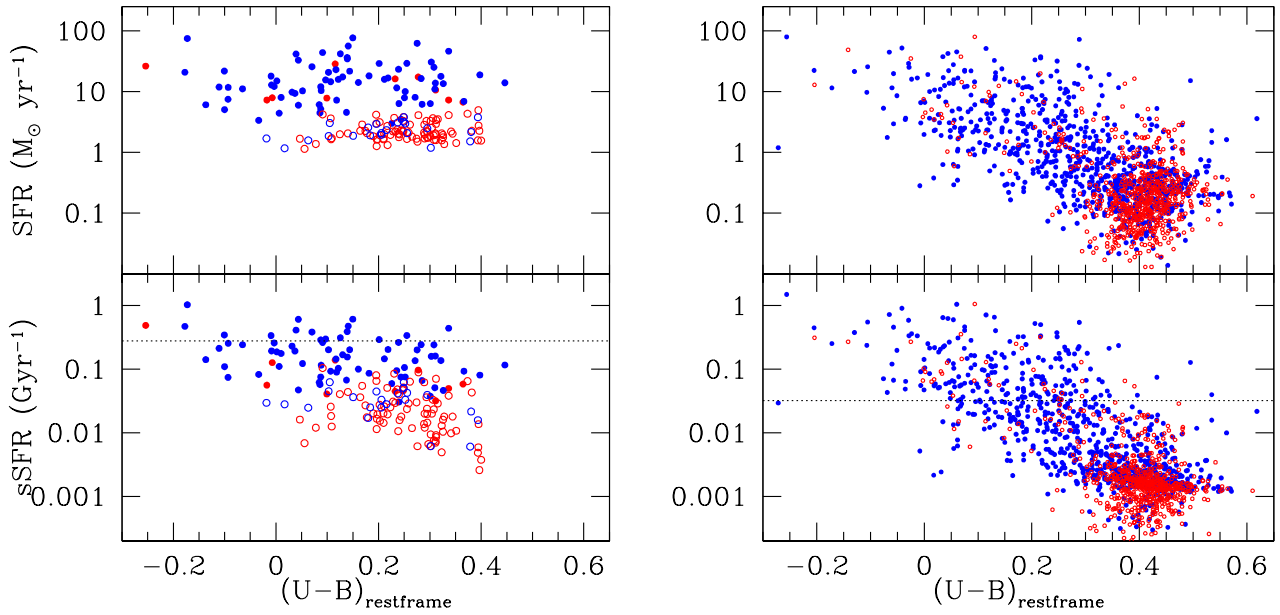


FIG. 11.— *Top left:* SFR (derived from 24 μm photometry) as a function of rest-frame color for the $z \sim 0.8$ sample. The red circles are early-type galaxies, the blue circles are late-type galaxies. Filled circles are objects with significant ($> 5\sigma$) 24 μm detections, open circles are objects without significant detections (upper limits are shown). *Bottom left:* For the same sample as in the top left panel, the specific SFR as a function of color. *Top right:* SFR (derived from modeling optical emission lines; Brinchmann et al. 2004) as a function of color for the $z \sim 0.03$ sample. Open red circles are early-type galaxies, and filled blue circles are late-type galaxies. *Bottom right:* For the same sample as in the top right panel, the specific SFR as a function of color. For both the low- and high-redshift samples, the star formation activity is low in early-type galaxies. SFRs are higher for late types, with a marked decrease in SFR for red late-type galaxies between $z = 0.8$ and the present. The dotted lines in the two bottom panels indicate the expected specific SFRs associated with galaxies that will double/have doubled their stellar masses between $z = 1$ and the present under the assumption that their SFRs decline (exponentially as a function of redshift) by an order of magnitude between $z = 1$ and the present. The decreased star formation activity in our $z \sim 0.03$ sample with respect to our $z \sim 0.8$ sample is consistent with the decline of the cosmic SFR.

within the spectroscopic fiber of the SDSS spectrograph. We use the stellar mass derived within the same fiber aperture (Kauffmann et al. 2003),[9] and scale the SFR, comparing the fiber stellar mass with our total stellar mass (§ 2.1). We show the SFR and specific SFR in Figure 11. The global trend is similar to that observed at $z \sim 0.8$, with early-type galaxies showing lower star formation activity than late-type galaxies.

It should be kept in mind that SFRs of the $z \sim 0.03$ galaxies are determined from optical emission lines as measured with a 3″ fiber, such that extended star formation can be missed, and a systematic difference between the total SFRs of the $z \sim 0.8$ galaxies is created. In addition, it is well known that IR-derived and emission- line-derived SFRs can be intrinsically different and depend on metallicity and the amount of extinction. Therefore, we have to restrict ourselves to the description and interpretation of evolutionary trends of at least an order of magnitude.

Despite the large uncertainties and the high upper limit of 5 $M_\odot$ yr^{-1} for the $z \sim 0.8$ sample, Figure 11 shows that the overall star formation activity decreases between $z \sim 0.8$ and the present (see also Table 1). One prominent difference between the $z \sim 0.03$ and ~ 0.8 samples is the marked decrease of star formation activity by 2 orders of magnitude in late-type galaxies that are located on the red sequence. In the local universe, their SFRs are as low as those of early-type galaxies, whereas at $z \sim 0.8$ their SFRs are at least an order of magnitude higher than those of the early types.

In Figure 11 we indicate the specific SFR expected for galaxies that double their stellar mass between $z = 1$ and the present, assuming an exponential decline in SFR by a factor of 10 over that period. Such a level of star formation, both at $z \sim 0.03$ and at $z \sim 0.8$, coincides with the typical specific SFR of late-type galaxies. The decrease in star formation activity as observed in our samples follows the cosmic average trend of decline by an order of magnitude since $z \sim 1$. At the same time, the morphological mix has remained unchanged, at least, if only two morphological classes are considered. These results are therefore not mutually exclusive and have to be reconciled with each other.

4.2. *The Red Sequence and the Evolution of the Stellar Mass Density*

In Figs. 12 we show the rest-frame $U - B$ color distribution as a function of stellar mass for the low- and high-redshift samples. The $U - B$ colors of the $z \sim 0.8$ sample are corrected for evolution within the sample redshift range $0.6 < z < 1.0$, assuming $\Delta(U - B) = 0.22(z - 0.8)$ (see below). This is a small effect of typically 0.02 mag. We define the early-type galaxy red sequence for the $z \sim 0.03$ sample by a linear fit, with the slope and the zero point as free parameters, and iteratively rejecting 3σ outliers (8% are rejected, virtually all blueward of the red sequence). In order to minimize systematic effects, we define the red sequence for the $z \sim 0.8$ sample with the same slope (0.08 mag dex^{-1}) and scatter (0.05 mag), with only the zero point as a free parameter. The red sequence for both samples is shown in Figure 12. Color

[9] The stellar masses and SFRs are publicly available at http://www.mpa-garching.mpg.de/SDSS/DR4/

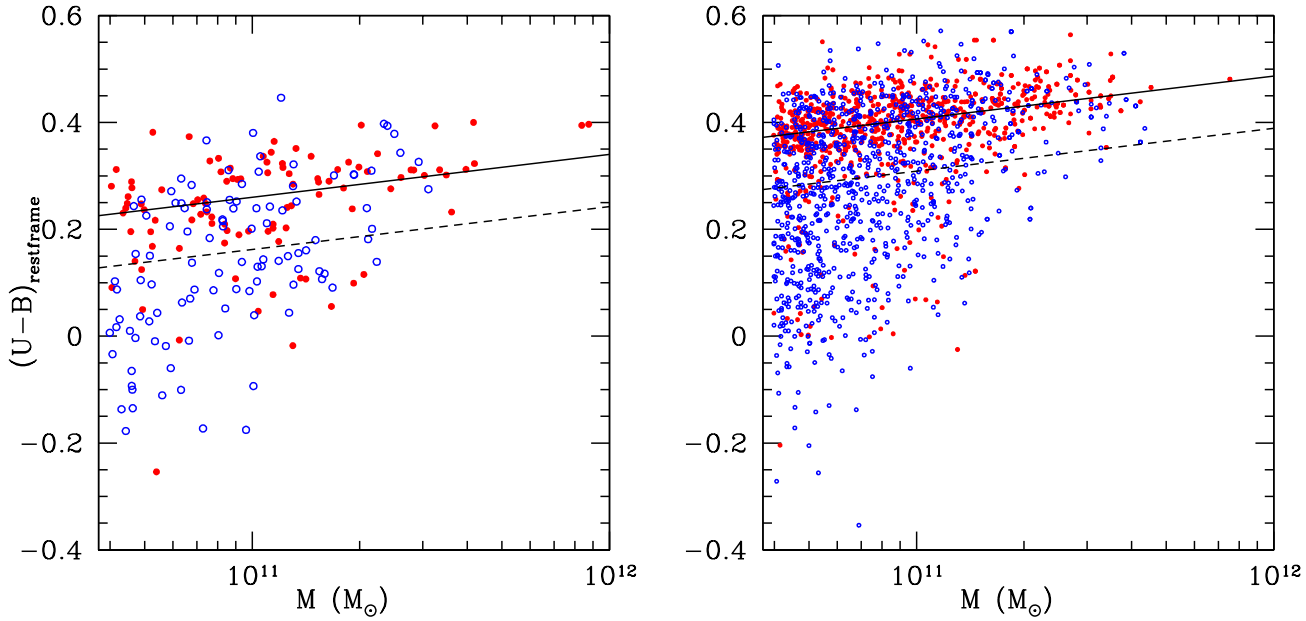


FIG. 12.— Stellar mass vs. rest-frame $U-B$ color for the $z\sim0.8$ sample (*left*) the $z\sim0.03$ sample (*right*). Early-type galaxies are indicated by filled red circles symbols, late-type galaxies by open blue circles. Color evolution is readily visible, with the red sequence being significantly bluer at $z\sim0.8$ than at $z\sim0.03$. The solid lines indicate the best fits to the red sequence as defined by the early-type galaxies, and the dashed lines separate blue and red galaxies (see text for an explanation). The relative numbers of red galaxies in the $z\sim0.03$ and ~0.8 samples are not significantly different (see also Table 1). In addition, the fraction of red galaxies with late-type morphologies is similar in both samples.

evolution between $z\sim0.8$ and ~0.03 of 0.15 mag, or 0.20 mag per unit redshift, is readily visible. We also fit the slope and scatter of the $z\sim0.8$ red sequence independently, resulting in a higher scatter (0.08 mag) and a steeper slope (0.11 mag dex^{-1}).

For both samples we define blue galaxies as galaxies with colors more than 2 σ below the red sequence (with $\sigma=0.05$ as defined above; see Fig. 12). With this definition, we find similar red-galaxy fractions of 64% and 68% for the $z\sim0.8$ and ~0.03 samples, respectively (see Table 1). Like the early-type fraction, the red-galaxy fraction shows no strong evolution with redshift. The red-galaxy fraction is significantly higher than the early-type fraction in both samples (see also Bundy et al. 2006). This is due to the presence of many late-type galaxies on the red sequence: $38\%\pm8\%$ for the $z\sim0.8$ sample and $45\%\pm3\%$ for the $z\sim0.03$ sample of the red galaxies are late types (see also Fig. 13). Conversely, in either sample less than 20% of the blue galaxies have early-type morphologies.

Given the fact that the majority of the galaxies in both our samples are located on the red sequence, our earlier conclusion that the early-type galaxy fraction at a given density does not evolve with redshift seems, at first sight, to be at odds with the observation that the stellar mass density of red-sequence galaxies has doubled since $z=1$ (e.g., Bell et al. 2004b; Brown et al. 2007). The luminosity limit for red galaxies at $z=1$ in our sample ($M_{\rm B}\sim-20$) is similar as that of, e.g., Bell et al. (2004b) and Brown et al. (2007); therefore, the increase in mass density found by those authors has to take place above the mass threshold of our samples. In fact, even in our samples, which cover only small volumes, we observe an increase in stellar mass density from $z=0.8$ to the present.

If the mass function of galaxies evolves, it is not entirely appropriate to compare galaxy samples at different redshifts down to the same mass limit. If galaxies evolve by a factor of 2 in stellar mass between $z=0.08$ and the present, the mass limit at $z=0.8$ should be chosen 0.3 dex lower than at $z=0$, otherwise many of the progenitors in the $z=0$ sample will not be included in the $=0.8$ sample. We test this effect by choosing a mass limit for our $z\sim0.03$ sample that is 0.3 dex higher ($M=8\times10^{10}\ M_\odot$) than for the $z\sim0.8$ sample. The early-type fraction increases slightly, from $43\%\pm3\%$ to $48\%\pm3\%$. Due to the errors it is not clear whether this agrees better with the $z\sim0.8$ early-type galaxy fraction ($48\%\pm7\%$), but it is striking that the values are the same.

We conclude that the growth of the red-sequence galaxy population must happen in such a way that the MDR is conserved. The accretion of red galaxies onto the red sequence and/or the growth of galaxies on the red sequence must preserve the relative number of late- and early-type galaxies with masses $M>4\times10^{10}\ M_\odot$. The galaxy population evolves along the MDR, whereas the MDR itself is a fixed relationship between environment and morphological appearance.

Since many star-forming, late-type galaxies are located on the red sequence, the stellar mass density of red-sequence galaxies will increase through *in situ* star formation. The question is how much this contributes to the observed increase in stellar mass density of red galaxies. If we make the assumption that the SFR of the galaxies in our $z\sim0.8$ sample decreases exponentially at the same rate as the cosmic average, i.e., by an order of magnitude between $z=1$ and the present, the average late-type galaxy on the red sequence will increase its stellar mass by $20\%-80\%$. The large uncertainty is caused by the absolute uncertainty in the IR-derived SFR of a factor of 2 (see § 4.1). Given such an increase in stellar

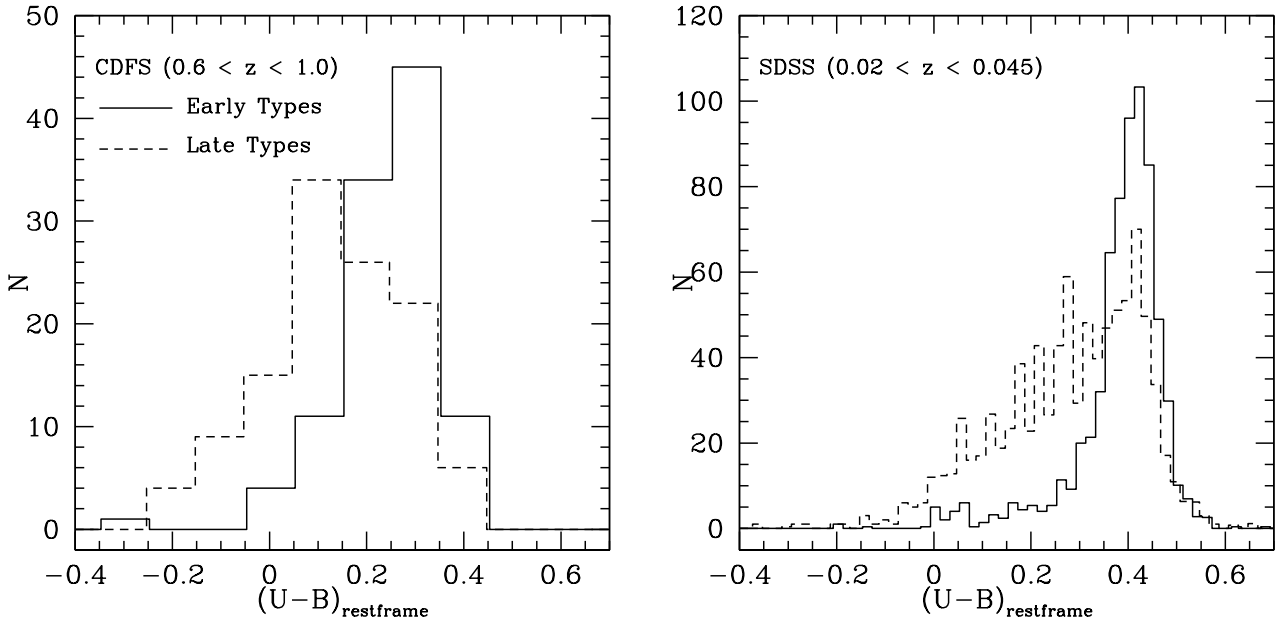


FIG. 13.— Rest-frame $U-B$ color distribution of the mass selected $z \sim 0.8$ (*left*) and $z \sim 0.03$ (*right*) samples. The solid lines indicate the early-type galaxies, and the dashed lines indicate the late-type galaxies. The relative numbers of red galaxies and the relative numbers of red galaxies with late-type morphologies are not significantly different at $z \sim 0.03$ and ~ 0.8.

mass, there will be galaxies that are below our mass cut-off at $z \sim 0.8$ but would not be during the present epoch. We can estimate this effect by calculating the total stellar mass in red, late-type galaxies in our $z \sim 0.03$ sample with masses less than $1.2-1.8$ times the threshold. Their contribution to the total stellar mass in red galaxies is $2\%-11\%$, such that the total increase in the stellar mass density through *in situ* star formation in red late types is a factor of $1.2-2$. This is close the observed evolution of a factor of $\sim$2. One caveat is the possible evolution with redshift of the color-M/L relation, which we use to estimate the stellar masses (see § 2.2). This may cancel out the growth in stellar mass as estimated above.

With the hypothesis that merging does not play a role in shaping the red sequence galaxy population, the above described process of star formation in late types, but not in early types, will change the morphological mix of a mass-selected sample of red galaxies. The early-type fraction will then decrease with time or increase with redshift. As mentioned in § 4.2, the fraction of early-type galaxies on the red sequence is indeed consistent with an increase from $z \sim 0.03$ to ~ 0.8 (from 55% to 62%). Even though this difference is not significant, at least it is consistent with a growth in stellar mass of late-type galaxies by a factor of 1.5.

These speculations depend on the assumption that a large reservoir of lower mass, red galaxies is available to provide the necessary growth of stellar mass through star formation on the red sequence. Given the evidence for the opposite, i.e., the lack of faint, red galaxies at significant look-back times (e.g., Tanaka et al. 2005; De Lucia et al. 2007), truncation of star formation in blue galaxies is possibly required to explain the growth of the red sequence. The above estimates of growth through *in situ* star formation merely serve as a cautionary statement to indicate that a factor of 2 evolution in the red-galaxy mass density is rather modest and can be accounted for in various ways.

Of course, if, for some reason, current measurements overestimate the evolution in the red-galaxy population, our results can be regarded as evidence for passive evolution of red galaxies, in terms of both star formation and mass assembly. We stress, however, that this is most likely not the case, given the mounting evidence for considerable evolution in the stellar mass density of red galaxies since $z = 1$.

4.3. *Comparison with Other Studies*

Numerous studies have analyzed the morphological and structural properties of galaxies in the local universe and at high redshifts. Even though it is not feasible to discuss all previous work, we put our work on the local galaxy population in the context of several other studies and compare our results with those from several recent efforts with the similar objective to measure the evolution with redshift of the early-type fraction outside massive clusters.

Goto et al. (2003) derive the MDR for luminosity-selected galaxies at $0.05 < z < 0.10$. Their morphological classifications are simply based on the concentration of the light profile, and they find early-type galaxy fractions of $\sim 40\%-60\%$ at low densities, depending on the strictness of the classification criterion for early types. This is consistent with our results. Goto et al. (2003) note that at densities below $\Sigma \sim 1$ Mpc^{-2} the early-type fraction changes less rapidly with density than at higher densities. This trend is even more pronounced in our mass-selected sample: at densities $\Sigma < 1$ Mpc^{-2} the early-type fraction is constant at $\sim 40\%$ and only increases at higher densities (see Fig. 10 and § 3.2).

The contributions of galaxies with different morphologies to the total stellar mass density have been measured by Bell et al. (2003), who find that nowadays 76% of the stars in galaxies more massive than $M = 4 \times 10^{10}\ M_{\odot}$ reside in early-type galaxies. In our $z \sim 0.03$ sample, we find a much lower value of 47%. The cause of this

difference is that Bell et al. use a single parameter (the concentration index) as a proxy for morphology, which corresponds with visual classifications 70% of the time (see also Strateva et al. 2001). Our method uses the bumpiness parameter B in addition to the PSF-corrected concentration of the light profile, quantified by the Sérsic parameter n. Thus, early-type galaxies are required to be not only highly concentrated but also smooth. This extension increases the agreement with visual classifications to ∼90% (see § 2.3). This improvement is not due to smaller random errors: the contribution to the total stellar mass density of highly concentrated galaxies in our $z \sim 0.03$ sample (those with $n > 2.5$) is 70%, in good agreement with the result by Bell et al. (2003), and higher than that of early-type galaxies as defined by both visual classifications and by our $B - n$ method. Many of the galaxies with $n > 2.5$ have late-type morphologies, which is only revealed through visual classifications or the use of an additional parameter such as bumpiness. As was demonstrated by Kauffmann et al. (2004), the concentration distribution of the galaxy population provides crucial insight into the formation and evolution of galaxies. However, this structural property should be distinguished from morphology. The latter is related to the smoothness of the light profile in addition to its concentration. It may well be that structure and morphology are correlated but distinct physical parameters that are affected by, e.g., galaxy mass and environment in different ways.

Recently, several studies have addressed the evolution with redshift of the morphological mix of field galaxies. Abraham et al. (2007) find that for galaxies more massive than $M = 4 \times 10^{10}\ M_{\odot}$ the fraction of the stellar mass density residing in early-type galaxies is ∼80% at $z \sim 1$, similar to the numbers from Bell et al. (2003) and our n-selected sample at low redshift. Abraham et al. use two parameters to distinguish early types from late types: in addition to the Gini coefficient (which, for early types and spiral galaxies, closely corresponds to the concentration index) they use asymmetry as a morphological indicator. However, the addition of asymmetry does not substantially improve the agreement with visual classifications for galaxies with type Sb or later (see, e.g., Conselice 2003). The method used by Abraham et al. (2007) therefore effectively classifies galaxies by concentration. In our $z \sim 0.8$ sample, highly concentrated galaxies (with $n > 2.5$) contribute 72% to the total stellar mass density, similar to what Abraham et al. find (∼80%). The stellar mass in early-type galaxies as defined by our $B - n$ method or visual classifications is lower (57%), consistent with the results by Bundy et al. (2005), which are also based on visual classifications. We conclude that the difference between our numbers and those from Abraham et al. (2007) are due to the difference between the classifying methods. Note that the relative early-type galaxy mass density does not evolve between $z \sim 1$ and the present, independent of the applied morphological classification method.

Capak et al. (2007), who use the Gini coefficient to determine morphologies, find a significant decrease with redshift (in the range $0.4 < z < 1.2$) of the early-type fraction in high-density regions (with $\Sigma > 100$ Mpc^{-2}). At lower densities (with $\Sigma < 50$ Mpc^{-2}) they find a constant early-type fraction between $z = 0.4$ and 1.2 that is consistent with the early-type fraction that we find. However, when they compare their results with the local early-type fraction, measured with different classification methods, they do find significant evolution, also at the lowest densities. The sample constructed by Capak et al. (2007) is selected by luminosity, and is therefore not directly comparable with our sample. As was demonstrated above, selecting early-type galaxies by Gini coefficient or concentration index alone overestimates the number of early-type galaxies as compared to visual classifications or our $B-n$ method. This, combined with the difference between luminosity- and mass-selected samples, may conspire to yield an early-type fraction similar to that we find for visually classified galaxies in a mass-selected sample.

We conclude that our results are either consistent with previous work or can be explained by the differences in approach. We note that the GOODS/ACS imaging that we use to determine galaxy morphologies at $z \sim 0.8$ is much deeper than then imaging used by Capak et al. (2007) and effectively as deep as the data used by Abraham et al. (2007) in terms of S/N for red galaxies at $z \sim 1$. Moreover, our study is the first of its kind to quantify galaxy morphologies in the local universe and at higher redshifts in an internally consistent manner.

5. SUMMARY

In this paper we examine the early-type galaxy (E+S0) fraction and its evolution for stellar-mass-selected, volume-limited samples of galaxies at redshifts $0 < z < 1$. At low redshift we estimate stellar masses and determine morphologies for 2003 galaxies at redshifts $0.02 < z < 0.045$ in the SDSS, complete down to a mass of $M = 4 \times 10^{10}\ M_{\odot}$, 60% of the mass of a typical (L_*) galaxy. In addition, we construct a similar sample of 207 galaxies in the CDF-S at redshifts $0.6 < z < 1.0$, complete down to the same mass limit. The stellar mass estimates are based on the relation between color and M/L, which has been proved to work without significant systematic effects with respect to kinematic mass measurements at low and high redshift. Morphologies are determined with an automated method, based on the Sérsic parameter and the bumpiness of the residual. We compare this method with the traditional visual classifications and find no systematic differences when we split the sample into two morphological classes (Sp+Irr and E+S0). We estimate the local surface density with an nth nearest neighbor method. The density for the galaxies in our samples is typically $\Sigma \sim 1$ Mpc^{-2} and ranges from ∼0.01 to 100 Mpc^{-2}. The sample characteristics are summarized in Table 1.

We find that for galaxies with masses higher than $M = 4 \times 10^{10}\ M_{\odot}$ the early-type fraction in the field and group environment probed by our samples has not changed significantly between $z = 0.8$ and the present. The early-type fraction is $43\% \pm 3\%$ for the $z \sim 0.03$ sample, and $48\% \pm 7\%$ for the $z \sim 0.8$ sample. When we combine this with the unchanging early-type fraction of $> 80\%$ in dense (> 100 Mpc^{-2}) cluster environments over the same redshift range and down to the same mass limit (Paper I), we find that the MDR has not evolved significantly between $z \sim 0.8$ and the present over at least 3 orders of magnitude in density.

In both our $z \sim 0.03$ sample and our $z \sim 0.8$ sample, $65\% - 70\%$ of the galaxies (see also Table 1) are located on the red sequence, in agreement with previous work. In addition, $65\% - 70\%$ of the galaxies in both samples have Sérsic indices $n > 2.5$. Our samples follow the well-constrained trends that the stellar mass density of red galaxies has increased and the global star formation activity has decreased between $z \sim 1$ and the present. In fact, star formation in red galaxies could contribute significantly to the growth in the stellar mass density of red galaxies without strong evolution in the early-type galaxy fraction.

Future work will include a more detailed analysis of the morphological mix, e.g., the separation of the late types into irregular and spiral galaxies and the separation of the early types into E and S0 galaxies. Furthermore, studies in larger fields with high-resolution imaging will be used to measure the shape of the MDR at low densities in more detail. In particular, it is important to study intermediately dense regions, i.e., the infalling regions around clusters. At those densities the morphological mix of the galaxy population appears to undergo the most rapid change as a function of density. A crucial step forward in understanding the role of the environment and the role of the internal properties of galaxies in shaping their stellar populations and morphologies will be to include the evolution of the density itself in analyses such as those carried out in this paper. Another challenge will be to establish at what redshift the MDR emerges, whether this coincides with the emergence of the red sequence, and how this relates to the buildup of the stellar mass function.

We thank the referee, Bob Abraham, for his thorough reading of the manuscript and positive feedback. We would like to thank Pieter van Dokkum for helpful suggestions and Sandy Faber for stimulating discussion. A. v. d. W. acknowledges support from NASA grant NAG5-7697.

REFERENCES

Abraham, R. G. et al. 2007, astro-ph/0704.1475
Abraham, R. G., van den Bergh, S., & Nair, P. 2003, ApJ, 588, 218
Adelman-McCarthy, J. et al. 2007, ApJS, 172, 634
Baldry, I. K., Balogh, M. L., Bower, R. G., Glazebrook, K., Nichol, R. C., Bamford, S. P., & Budavari, T. 2006, MNRAS, 373, 469
Bell, E. F. et al. 2004a, ApJ, 600, L11
Bell, E. F., McIntosh, D. H., Katz, N., & Weinberg, M. D. 2003, ApJS, 149, 289
Bell, E. F. et al. 2005, ApJ, 625, 23
Bell, E. F. et al. 2004b, ApJ, 608, 752
Benítez, N. et al. 2004, ApJS, 150, 1
Bernardi, M. et al. 2003, AJ, 125, 1817
Bertin, E., & Arnouts, S. 1996, A&AS, 117, 393
Blakeslee, J. P. et al. 2006, ApJ, 644, 30
Blanton, M. R. et al. 2003, AJ, 125, 2348
Blanton, M. R., Eisenstein, D., Hogg, D. W., Schlegel, D. J., & Brinkmann, J. 2005a, ApJ, 629, 143
Blanton, M. R., Lupton, R. H., Schlegel, D. J., Strauss, M. A., Brinkmann, J., Fukugita, M., & Loveday, J. 2005b, ApJ, 631, 208
Brinchmann, J., Charlot, S., White, S. D. M., Tremonti, C., Kauffmann, G., Heckman, T., & Brinkmann, J. 2004, MNRAS, 351, 1151
Brown, M. J. I. et al. 2007, ApJ, 654, 858
Bruzual, G., & Charlot, S. 2003, MNRAS, 344, 1000
Bundy, K., Ellis, R. S., & Conselice, C. J. 2005, ApJ, 625, 621
Bundy, K. et al. 2006, ApJ, 651, 120
Capak, P. L., Abraham, R. G., Ellis, R. S., Mobasher, B., Scoville, N. Z., Sheth, K., & Koekemoer, A. 2007, astro-ph/0703668
Chary, R., & Elbaz, D. 2001, ApJ, 556, 562
Conselice, C. J. 2003, ApJS, 147, 1
Conselice, C. J., Bershady, M. A., & Jangren, A. 2000, ApJ, 529, 886
De Lucia, G. et al. 2007, MNRAS, 374, 809
De Propris, R., Stanford, S. A., Eisenhardt, P. R., Holden, B., & Rosati, P. 2007, AJ, 133, 2209
Desai. V. et al. 2007, ApJ, 660, 1151
Dressler, A. 1980, ApJ, 236, 351
Dressler, A. et al. 1997, ApJ, 490, 577
Faber, S. M. et al. 2007, ApJ, 665, 265
Fazio, G. G. et al. 2004, ApJS, 154, 10
Goto, T. et al. 2003, MNRAS, 346, 601
Hogg, D. W. et al. 2003, ApJ, 585, L5
Holden, B. P. et al. 2006, ApJ, 642, L123
Holden, B. P. et al. 2007, ApJ, 670, 195
Jørgensen, I., Franx, M., & Kjaergaard, P. 1996, MNRAS, 280, 167
Juneau, S. et al. 2005, ApJ, 619, L135
Kassin, S. A. et al. 2007, ApJ, 660, 35
Kauffmann, G. et al. 2003, MNRAS, 341, 33
Kauffmann, G. et al. 2004, MNRAS, 353, 713
Kennicutt, R. C. 1998, ARA&A, 36, 189
Lauer, T. R. et al. 2007, ApJ, 662, 808
Le Fèvre, O. et al. 2004, A&A, 428, 1043
Le Floc'h, E. et al. 2005, ApJ, 632, 169
Lotz, J. M., Primack, J., & Madau, P. 2004, AJ, 128, 163
Lupton, R., Gunn, J. E., Ivezić, Z., Knapp, G. R., & Kent, S. 2001, in ASP Conf. Ser. 238: Astronomical Data Analysis Software and Systems X, ed. F. R. Harnden, Jr., F. A. Primini, & H. E. Payne, 269—+
Madau, P., Ferguson, H. C., Dickinson, M. E., Giavalisco, M., Steidel, C. C., & Fruchter, A. 1996, MNRAS, 283, 1388
Mignoli, M. e al. 2005, A&A, 437, 883
Noeske, K. G. et al. 2007, ApJ, 660, L43
Peng, C. Y., Ho, L. C., Impey, C. D., & Rix, H.-W. 2002, AJ, 124, 266
Pérez-González, P. G. et al. 2005, ApJ, 630, 82
Postman, M. et al. 2005, ApJ, 623, 721
Rieke, G. H. et al. 2004, ApJS, 154, 25
Smith, G. P., Treu, T., Ellis, R. S., Moran, S. M., & Dressler, A. 2005, ApJ, 620, 78
Strateva, I. et al. 2001, AJ, 122, 1861
Strauss, M. A. et al. 2002, AJ, 124, 1810
Tanaka, M. et al. 2005, MNRAS, 362, 268
Treu, T. etal. 2005, ApJ, 633, 174
Treu, T. et al. 2003, ApJ, 591, 53
van der Wel, A., Franx, M., van Dokkum, P. G., Rix, H.-W., Illingworth, G. D., & Rosati, P. 2005, ApJ, 631, 145
van der Wel, A., Franx, M., Wuyts, S., van Dokkum, P. G., Huang, J., Rix, H.-W., & Illingworth, G. 2006, ApJ, 652, 97
van der Wel et al. 2007, astro-ph/0705.3394
van Dokkum, P. G., & van der Marel, R. P. 2007, ApJ, 655, 30
Vanzella, E. et al. 2006, A&A, 454, 423
von der Linden, A., Best, P. N., Kauffmann, G., & White, S. D. M. MNRAS, 379, 867
Wolf, C., Meisenheimer, K., Rix, H.-W., Borch, A., Dye, S., & Kleinheinrich, M. 2003, A&A, 401, 73
Wuyts, S. et al. 2007, ApJ, 655, 51
York, D. G. et al. 2000, AJ, 120, 1579
Zheng, X. Z., Bell, E. F., Rix, H.-W., Papovich, C., Le Floc'h, E., Rieke, G. H., & Pérez-González, P. G. 2006, ApJ, 640, 784